EXPERIMENTAL INVESTIGATION OF PERFORMANCE OF VINH-HOUMAIRE WIND TURBINE

A thesis submitted

in partial fulfillment of the requirements

for the Degree of

MASTER OF TECHNOLOGY

by

KURADE RAJAN BHARAT

DEPARTMENT OF AEROSPACE ENGINEERING

IIT KANPUR

JUNE 2004

CERTIFICATE

It is certified that the work contained in the thesis titled **"EXPERIMENTAL INVESTIGATION OF PERFORMANCE OF VINH-HOUMAIRE WIND TURBINE"** by **"KURADE RAJAN BHARAT"** has been carried out under our supervision and that this work has not been submitted elsewhere for a degree.

Dr. Kunal Ghosh

Professor,

Department of Aerospace Engineering,

I. I. T. Kanpur,

Kanpur – 208 016.

for **Dr. Debopam Das**

Assistant Professor,

Department of Aerospace Engineering,

I. I. T. Kanpur,

Kanpur – 208 016.

ABSTRACT

Vinh and Houmaire tested a Vertical Axis Wind Turbine which is somewhat akin to a Savonius rotor. Their wind turbine consists of three pairs of semicircle and flat plate. These pairs are placed 120^0 apart between two circular discs. The flat plate is kept on the concave side of the semicircle normal to the diameter so that it directs the oncoming flow into the semicircular cup.

The Savonius suffers from certain disadvantages. It has to be supported from the top end and this results in a more expensive tower. However the most significant disadvantage is that the torque goes through wide variation when plotted against wind angle. Twice in a cycle (0 to 360^0) it actually becomes slightly negative. The Vinh-Houmaire turbine is likely to have a more uniform torque because of its geometry; however, its torque characteristics have not been reported by the inventors.

A model of this turbine is tested in Wind Tunnel Facility of I .I .T. Kanpur which has a large test section (3 m $\times$ 2.25 m). This allows testing of large models reaching upto a maximum Reynolds number of 8.87×10^5. The forces and moments generated at different wind speeds are recorded with the help of a wind tunnel balance. Power is measured with the help of a device similar to a Brake - dynamometer and wind tunnel balance. The coefficient of power shows a maximum of 0.11 at a tip speed ratio of 0.36 and coefficient of torque shows a maximum of 0.42 at a tip speed ratio between 0 and 0.15. The coefficient of power seems to be well below that claimed by Vinh and Houmaire which is 0.32 at a tip speed ratio of 0.7. Torque is more uniform over a cycle of rotation compared to a Savonius rotor.

Keywords: Vertical axis wind turbine, Brake-dynamometer, Power coefficient, Torque coefficient, Tip speed ratio.

Dedicated to my Parents, Brother and Sister.

ACKNOWLEDGEMENT

A person's life and work are shaped by, besides his own thoughts and efforts, the influence of people surrounding him. In my life's journey so far, many individuals have contributed in my overall development at various stages and in different ways. At this juncture, I wish to express my gratitude towards them.

First of all I pay my heartiest regards to Almighty God who has given me energy and enthusiasm throughout my life to come at this stage. I always seek his blessings.

It is indeed with a deep sense of gratitude that I express my sincere regard to my guide Dr.Kunal Ghosh for his invaluable guidance, constructive suggestions, encouragement and moral support at every stage of this work. A special note of thanks and sincere regards to my coguide Dr.Debopam Das for encouraging me and for being with me during experiments under all odd conditions. He really boosted me in all the difficult and confusing situations. I would be always greatful to Dr.Kamal Poddar and NWTF staff for their invaluable help for the experiments in NWTF. I must pay my regards to all staff members of Department of Aerospace Engineering, workshop , Mr. Sanjeev Gupta and Miss. Vijaya Kirti Gupta. It was really difficult to complete this work without their involvement.

Life at IIT Kanpur has been a roller coaster ride, full of myriad experiences. The period of stay on this campus has helped me know myself better. The vibrant atmosphere the state-of art facilities, the excellent infrastructure and spirit of excellence at IIT kanpur are unmatched and definitely deserve a mention.

A special note of thanks and appreciation for my friends who really stood behind me and made this work possible. They added a new dimension to my life and brought me in

contact with many interesting persons. Were it not for my friends, life here would have been dull and boring. It gives me immense pleasure to recall my association with Ritesh, Nandu, Sai, Vivek, Papa Rao, Sreejith, Gautam, Ashvin, Gaurav, Nilesh, Ravindra, Amit and Aniruddha. I would be also greatful to my Marathi family here in IIT Kanpur especially Amita, Gayatri, Sagar and Sushil for their love and affection for me. They were with me whenever I needed them. They made me to feel at home. Everything and everybody made my stay at IIT kanpur memorable. Three cheers for IIT kanpur and its campus community.

Last but not the least, I wish to record my heartiest regards and reverence to my beloved parents, brother and sister for their deep affection, moral support, pains-taking assistance, constant encouragement and blessing for achieving goals. This is nothing in return what they have given me.

RAJAN KURADE

Contents

List of Figures

List of Tables

Chapter 1

INTRODUCTION AND LITERATURE REVIEW

1.1 INTRODUCTION

The wind is free, clean and inexhaustible energy source. It has served human kind well for many centuries by propelling ships and driving wind turbines. Introduction of coal, petroleum or nuclear energy has changed the energy consumption pattern and quality of life. Nuclear energy appeared in the energy supply scene in fifties with a great promise. In just three decades this latest energy source of unbound potential has been besieged with problems of waste disposal, radiation hazard and safety.

The growing demand as well as shortage of conventional sources of energy is going to create a crisis, as the fossil fuels are exhaustible and sufficient power will not be produced using these conventional source of energy in near future. Now the world is trying a way out of a situation through a greater reliance on non-conventional form of energy, in particular the renewable such as solar, wind, tidal, wave energy etc.

From ancient times human beings are using these renewable forms of energy. The wind

has been used to power sailing ships for many centuries. Indeed, wind was almost the only source of power for ships until Watt invented steam engine in the nineteenth century. On land too wind turbines or windmills have been used for long. Over the last 2000 years or more many types of wind machines have been invented.

1.2 THE HISTORY OF WIND POWER

Man has applied the technology of transforming the kinetic energy of the wind into useful mechanical power since antiquity. Anemometer type wind mills and water wheel are the oldest source of power.

The use of wind power is said to have its origin in the Asian civilization of China, Tibet, India, Afghanistan and Persia. The first written evidence for the use of wind turbines are that of Hero Of Alexandria, who in the second or third century BC described a simple horizontal axis wind turbine. It was described as giving power to an organ. From historical records we know that in the 7th century B. C. the persians seriously used wind power from a vertical axis machine (Johnson,1985).

From Asia the use of wind power spread to Europe. From contemporary sources we know that windmills have been used in the 11th or 12th century in England. Also from historical records(1190)we know that German crusaders brought the skills of building windmills to Syria. From this, we may assume that this technology was generally known all over Europe since the Middle Age.

The windmills and the water wheels are used in many under developed parts of the world for simple low energy processes such as water pumping and grain grinding. Since the first descriptions of windmills the technology developed over the centuries with some variations

from place to place. We all know the famous Dutch windmills used for water pumping, and in the Mediterranean area several islands are known for their old picturesque windmills.

With the introduction of the steam engine in the 19th century the world gradually changed its demand for power to techniques and machines based on thermodynamic processes. Especially with the introduction of fossil fuel (coal, oil and gas) the advantages of these machines become obvious. These new machines provided a more reliable source of power than wind turbines.

Therefore, the importance of wind energy as a power source decreased during the 19th century and especially during the present century, though in some parts of the world wind energy continued to be utilized. In countries with population scattered over large areas, such as the America, Australia, Russia, USSR wind power continued to contribute to the power needed by, for example farming. The American Jacobs brothers produced from 1925 to 1957 battery charging wind turbines in the range of 2.5 and 3 Kw in large numbers, and by the middle of this century the Aermotor company of Chicago claimed to have 800,000 windmills in service mostly for water pumping. These machines were built since the end of the 1890's and were made by steel.

Research in construction of wind turbines continued to a wider extent than normally assumed. Some of the highlights are the turbines of two Danes P, La Cour (around the turn of the century) and J. Juul (after world war II). In America the famous 1250 Kw Smith-Putnam wind turbine was erected as a place in Vermont called Granpa's Knob.

Meanwhile the traditional windrose-the multibladed wind turbine used in the farmland all over the world was still further developed and refined. Iron and steel replaced the wood used in most parts of these machines. Lattice steel towers were introduced and even steel

blades came into use.

In the 1920's and 30's the French F. M. Darrieus and the Finnish S. J. Savonius designed and tested new concepts for vertical axis machines. In the 1980's the Canadian firm Flowind mass-produced vertical axis wind turbines using the concept of Darrieus. These Darrieus turbines were a significant element in the Californian wind farms untill recently.

Development of theoretical work started. La Cour made some path-breaking empirical observations by using a primitive wind tunnel. In the 20's the German professor Albert Betz of the German aerodynamical research center in Gottingen made some path-breaking theoretical studies on wind turbines. Also in the 1920's H. Glauert contributed with an aerodynamic theory for wind turbines. Both of these theoretical contributions are still the foundation of today's rotor theory. Sandia laboratories, New Mexico has done extensive experiments on performance of two and three bucket Savonius rotor (Blackwell,1977).

A UNESCO conference on wind and solar energy was held in New Delhi in October 1954, and a world power conference was held in Brazil in July 1954. In 1961 a "United Nations Conference on New Sources of Energy" was held in Rome. The proceedings from this conference was published in 1964, and it contains key sources of information of the international development in wind power utilization in the first half of this century.

Hence research in wind power utilization did not die due to the competition of fossil fuels, and the revival of the wider interest in wind power after the 1970's did not start from scratch, but could build on a solid foundation of theories and practical experiences.

Above we mentioned the transition from wood to steel as the most dominant material. When the new era of wind energy was initiated in the 1970's new materials and technologies were available. Composite materials such as fiberglass, aluminium, reinforced plastic or steel

and laminated wood-epoxy showed to be very suitable for the blades. To make blades of medium and large wind rotors, fiberglass is generally favored by manufacturers. Aluminium alloy in the form of extruded bars is also common used in the construction of small wind machines (Le Gourieres,1982).

1.3 WIND MILLS

It is a machine that converts wind into useful energy. This energy is derived from the force of wind acting on oblique blades or sails through a rotating shaft. The turning shaft may be connected to machinery used to perform such work as milling grain, pumping water, or generating electricity. When the shaft is connected to a load, such as a pump, the device is typically called a windmill. When it is used to generate electricity, it is known as a wind turbine generator. Now a days both these names are used in a general sense.

Most powerful windmill stations which have been built are based on the horizontal axis system.This type of machine is classified as,

- the classic windmills
- the slow wind turbines
- the fast wind turbines

But this type of machines suffers from certain disadvantages like it has a very low starting torque. It has a high weight and material cost. Also the gear box and generator is placed on top of tower hence it requires bulky and expensive tower.It needs a yaw mechanism to turn the rotor into the wind and complicate control and storm security devices.

Vertical axis wind turbines can claim the distinction of being the forerunners to all wind machines. These are classified as,

- differential drag machines
- screened machines
- machines with flapping blades
- machines with turning blades
- machines with fixed, movable or cyclic pitch blades.

In present work we have studied the performance of Vinh-Houmaire vertical axis wind turbine.

1.4 Introduction to vertical axis wind turbine

Based on operating principle Vertical axis wind turbine (VAWT) designs can be classified as lift based design and drag based design. Drag based designs work like a paddle used to propel a canoe through the water. If you assume that the paddle used to propel your canoe did not slip, then your maximum speed would be about the same speed you drag your paddle. The same holds for the wind. The three cup anemometer commonly used for measuring wind speed are drag based vertical axis wind turbines. If the velocity of the cups is exactly the same as the wind speed, we can say that the instrument is operating with a tip speed ratio (TSR) defined as turbine tip speed to wind speed (denoted by λ) of 1. The ends of the cups can never go faster than the wind, so the λ is always 1 or less.

A good way of determining whether a VAWT design is based on drag or lift is to see if the λ can be better than 1. λ above 1 means some amount of lift, while λ below 1 means mostly the drag. Lift based designs can usually extract much power more efficiently.

1.4.1 The Savonius: drag-type VAWT

Although λ is not 1 still drag based VAWT can be useful. They can be made in many different ways with buckets, paddles, sails and oil drums. The Savonius rotor is s-shaped (when viewed from top) and apparently originated in Finland. A good Savonius turbine might exceed a TSR of 1, but not by much. All of these designs turn relatively slowly but yield a high torque. They can be useful for grinding grain, pumping water and many other tasks; but not good for generating electricity. RPM above 100 are generally best for producing electricity. However drag based VAWT usually turn below 100 RPM. One might use a gearbox but then the efficiency suffers and the machine may not start at all easily.

1.4.2 The darrieus: lift-type VAWT

There are also lift based VAWT like the "eggbeater". Darrieus from France first patented it in 1927. Each blade sees maximum lift(torque) only twice per revolution, making for a low torque (and power) sinusoidal output. And the long VAWT blades have many natural frequencies of vibration that must be avoided during operation.

1.4.3 Other lift-type vertical axis configurations

Darrieus' 1927 patent also covered machines with straight vertical axis blades called Giromills. A variant of Giromill called the cycloturbine uses a wind vane to mechanically orient a blade

pitch change mechanism.

There are not many easy to find references devoted to VAWT. The wind energy group of Sandia National Labs in Albuquerque, New Mexico has done a lot of research on Darrieus vertical axis technology. Straight bladed VAWT were explored by the National Wind Technology Center at NREL (Johnson,1985).

1.4.4 Advantages of vertical axis wind turbines

Advantages of Vertical Axis Wind turbines are as follows,

1. The generator, gearbox etc. are placed on the ground and that's why there is no need of a tall tower for the machine.

2. There is no need of a yaw mechanism to turn the rotor into the wind i.e. VAWT are Omnidirectional.

3. Due to the above fact VAWT's have a fixed pitch and low solidity.

4. Usually a very high tower for mounting is not required. This may be mounted on a small tower with help of guy wires. Such turbines can be used for household usages.

5. VAWT's do not have the cyclic varying stresses that the blades of HAWT experiences due to their own weight thus the chances of fatigue failure is low. These cyclic varying gravity stresses become progressively more dominant as the overall turbine size increases, and imposes a theoretical limit on the size of the horizontal axis rotor. Although VAWT blades experience cyclic varying aerodynamic loads, the resulting stresses remains substantially constant as the turbine size is increased.

1.4.5 Disadvantages of vertical axis wind turbines

1. Wind speeds are low close to ground level. So although one may save a little on a tower, the wind speeds will be low on the lower part of the rotor.

2. Darrieus type rotor are not self starting. These must be coupled with Savonius or must be pushed to start.

3. VAWT's are very difficult to mount high on a tower to capture the higher level winds. Because of this, they are usually forced to accept the lower, more turbulent winds and produce less power in possibly more damaging winds.

4. Guy cables are usually used to keep the turbine erect. They also impose a large thrust loading on the main turbine bearings and bearing selection is critical like all types of turbines, replacing main bearings requires that the turbine be taken down.

1.5 Review of theory

Performance of wind turbine rotors are determined through the estimation of torque and power coefficient. The power coefficient tells us how efficiently a turbine converts the energy in the wind into mechanical or electrical energy. Very simply, it is ratio of power by the wind energy input.At low wind speeds efficiency is not as important because there is not much energy to harvest. By design, at high wind speeds, the turbine wastes excess energy above generator rating. Torque coefficient is ratio of dimensional torque and free stream dynamic pressure, projected area and radius of turbine.

1.5.1 Power Vs wind speed curve

The speed at which wind turbine starts producing power is called Cut-in speed. Normally Cut in speed is about 3.5 m/s. Power varies with the cubic of wind speed. The speed at which the power is made constant is called as rated speed. This is about 11 m/s. The power corresponding to this speed is the rated wind power of the turbine. The speed at which the turbine is halted, disengaged or brakes are applied is called as Cut-out speed of the turbine. This is about 25 m/s. The maximum wind speed which can be withstood by the turbine is called as the Survival speed and is it is about 45-55 m/s. (Refer Figure 1).

1.5.2 Drag translator

Probably the simplest machine for extracting power from wind is a drag translator as shown in fig 2. Consider a cup shaped bluff body moving with a velocity 'v' relative to a wind speed of 'V'. The body moves in a straight line in the direction of wind. The swept area 'S' is independent of the velocity 'v'. The bluff body has a large wake and hence drag is maximized. This is the simplest arrangement for extracting power.

$$\begin{aligned} \text{Relative velocity} &= (V - v) \\ Drag = D &= C_D \times 0.5 \times \rho \times S \times (V - v)^2 \\ Power = P &= D \times v = C_D \times 0.5 \times \rho \times S \times (V - v)^2 \times v \\ \therefore P &= P(v) \end{aligned}$$

For maximum and minimum values of P

$$\frac{dP}{dv} = 0$$

Maximum power occurs when $v = V/3$.

Minimum power occurs when $v = V$.

$$\therefore P_{max} = \frac{2 \times C_D \times \rho \times S \times V^3}{27}$$

Let Power coefficient $= C_P$

$$C_{P_{max}} = \frac{P_{max}}{0.5 \times \rho \times S \times V^3}$$
$$\therefore C_{P_{max}} = \frac{4}{27} \times C_D$$

For cup shaped bluff body $C_D = 1.1 - 1.2$.

$$C_{P_{max}} = \frac{4}{27} = 0.14$$

1.5.3 LIFT TRANSLATOR

A lift translator is designed based on the aerodynamic shape of the blades. In this case the element moves perpendicular to the wind. The work is done by lift as motion is opposed by drag. (See figure 3).

V=velocity of wind.

v =velocity of the body.

α=angle between v and V

c=chord, width(span)

As v increases L and D vary with the relative wind.

$$cos\alpha = \frac{V}{\sqrt{(V^2 + v^2)}}$$
$$sin\alpha = \frac{v}{\sqrt{(V^2 + v^2)}}$$
$$\therefore \quad P = 0.5 \times \rho \times c \times 1 \times V^2 \times (C_L cos\alpha - C_D sin\alpha) \times v$$

Substitute $E = \frac{L}{D}$ = Efficiency of aerofoil = $\frac{C_L}{C_D}$ and $R = \frac{v}{V}$ = Speed ratio

$$
\begin{aligned}
P &= 0.5 \times \rho \times c \times (1 - \frac{R}{E}) \times R \times (1 + R^2) \\
\therefore C_P &= \frac{P}{(0.5 \times \rho \times c \times V^3)} \\
\therefore C_P &= C_L \times (1 - \frac{R}{E}) \times R \times (1 + R^2) \\
C_P &= C_P(R, C_L, E) \\
Set \quad \frac{dC_P}{dR} &= 0 \\
\therefore R &= (E + \sqrt{E^2 - 8})/4
\end{aligned}
$$

E = 30-40 for aerofoil

When $E^2 >> 8$, R $\equiv$ E/2

$$\therefore C_{P_{max}} = C_L \times E/4$$

1.5.4 Comparison of lift and drag translator

1. Lift translator can operate at V > v. Drag translator can not.

2. Torque is usually high for drag translator.For the sake of comparison take C_L=C_D=1

   For a lift translator $C_{P_{max}} = \frac{E}{4}$.

   For a drag translator $C_{P_{max}} = \frac{4}{27}$.

   $$\frac{(P_{max}/lift)}{(P_{max}/drag)} = \frac{27}{16} \times E.$$

   Since E>40 , the above ratio is 60.

   $\therefore$ Drag torque > Lift torque

3. The lift translator is difficult to design and maintain hence it is costly.

1.5.5 RANKINE-FROUDE ACTUATOR DISC THEORY

The rotor is replaced by an actuator disc through which the static pressure decreases discontinuously. This theory is based upon the following assumptions. (Refer Figure 4).

1. Steady, homogeneous wind
2. No obstruction to wind flow either upstream or downstream.
3. The flow velocity at disc is uniform.
4. Incompressible fluid.
5. No rotation of flow produced by disc.
6. Wind flow passing through disc is separable from remaining flow by well defined streamtube.

Assumption (3) requires that disc slow the wind equally at each radius, which is equivalent to assuming uniform thrust load.

Now consider the flow diagram (Refer Figure 4) of a cylindrical control volume of cross sectional area 'S'. Wind approaches the rotor at velocity V_0 far upstream at station 0 at ambient(static) pressure P_0. The rotor extracts energy and the reduced velocity causes the streamline to expand. If the velocity decrease induced by the rotor is 'v', then the velocity at the disc is $V_0 - v = u$. While far downstream at station 1 the wind has been slowed further to velocity u_1 and the pressure has returned to P_0. Let 'A' be the area of the rotor disc and the ρ be the air density. The momentum loss of the fluid is the result of the thrust 'T' that the rotor exerts against the flow, combined with the net resultant of the external pressure

on the control volume. Since the ambient atmospheric pressure P_0 acts on the entire control volume, it's net resultant is zero.

Within the streamtube, from continuity equation:

$$V_0 A_0 = uA = u_1 A_1$$

Writing continuity equation for the flow outside the streamtube between sections 0 and 1. We find that there must be a net flow δQ outside the control volume which is equal to,

$$\delta Q = V_0[(S - A_0) - (S - A_1)] = V_0(A_1 - A_0) \tag{1.1}$$

Writing the momentum theorem for the cylindrical control volume, we obtain

$$\rho V_0^2 S - T = \rho V_0^2 (S - A_1) + \rho u_1^2 A_1 + \rho \delta Q V_0 \tag{1.2}$$

Substituting δQ from Eqn(1.1) and $V_0 A_0 = u_1 A_1$ gives the thrust as

$$T = \rho A_1 u_1 (V_0 - u_1) \tag{1.3}$$

Physically, an actuator disc could be approximated by a rotor with a large number of very thin, drag less blades rotating with a tip speed much higher than the wind speed.

Applying the Bernoulli's equation from section 0 to section 3 and again from section2 to section 1, we have

$$\frac{1}{2}\rho V_0^2 + P_0 = \frac{1}{2}\rho u^2 + P_3 \tag{1.4}$$

$$\frac{1}{2}\rho u^2 + P_2 = \frac{1}{2}\rho u_1^2 + P_0 \tag{1.5}$$

The thrust on the rotor is then,

$$T = A(P_3 - P_2) \tag{1.6}$$

Solving for the pressure difference using Eqs. (1.4) and (1.5) gives,

$$T = \frac{\rho A(V_0^2 - u_1^2)}{2} \tag{1.7}$$

Equating Eqs. (1.3) and (1.7) and using $Au = A_1 u_1$, we find that,

$$u = \frac{(V_0 + u_1)}{2} \tag{1.8}$$

Thus the velocity at the disc is the average of the upstream and downstream velocities. Defining an axial interference factor 'a' as the fractal decrease in wind velocity between the free stream and the rotor plane represented by,

$$a = \frac{v}{V_0} \tag{1.9}$$

We find that,

$$u = V_0(1 - a) \tag{1.10}$$

Also

$$u_1 = V_0(1 - 2a) \tag{1.11}$$

The energy removed by the rotor per unit time is,

$$P = \frac{1}{2}\rho V_0^2 Au - \frac{1}{2}\rho u_1^2 Au = \frac{1}{2}\rho Au(V_0^2 - u_1^2) \tag{1.12}$$

$$\therefore P = \frac{1}{2}\rho Au(V_0 - u_1)(V_0 + u_1) \tag{1.13}$$

Substituting u from Eqn 1.11, we find that,

$$P = \frac{1}{2}\rho A V_0^3 4a(1 - a)^2 \tag{1.14}$$

We define a power coefficient, $C_P = \frac{P}{(\frac{1}{2}\rho A V_0^3)}$

so that,

$$C_P = 4a(1-a)^2 \tag{1.15}$$

Obtaining a maximum C_P as a function of 'a' gives $a = \frac{1}{3}$ so that,

$$C_{P_{max}} = \frac{16}{26} \equiv 0.59259 \tag{1.16}$$

$$u = (\frac{2}{3})V_0 \tag{1.17}$$

$$u_1 = (\frac{1}{3})V_0 \tag{1.18}$$

Additional data that can be derived from this model include the thrust loading on the rotor. The thrust on the rotor is(see Eqn(1.7))

$$T = \rho A \frac{(V_0^2 - u_1^2)}{2} \tag{1.19}$$

which for $u_1 = V_0(1-2a)$ simplifies to,

$$T = \frac{1}{2}\rho V_0^2 A[4a(1-a)] = qA[4a(1-a)] \tag{1.20}$$

where q is dynamic pressure.

On the other hand, if we were thinking of the rotor as a propeller, we would define a thrust coefficient as follows,

$$C_T = \frac{T}{qA} \tag{1.21}$$

$$\therefore C_T = 4a(1-a) \tag{1.22}$$

1.5.6 Qualitative theory of Vinh - Houmaire rotor

The Vinh - Houmaire rotor is primarily a differential drag rotor. The drag on the reverse or concave part of the cup is greater than the drag on the obverse or convex part. This

difference in drag gives a torque. When downstream of cup, the flat plate acts as a splitter plate and reduces drag (Rathakrishnan,1999). When it is upstream the flat plate deflects flow onto cup. The flat plate receives lift at certain angles and adds to the torque. At any orientation there are atleast two aerofoils giving positive torque. The torque is always unidirectional unlike the original Savonius rotor.

No quantitative theory is available for explaining the performance of modified Savonius rotor.

1.6 PRESENT WORK

We have studied Vinh-Houmaire turbine which consists of three pairs of semicircle and flat plate placed 120^0 apart between two circular discs.(See figure 5 and 6) The flat plate is kept on the concave side of semicircle normal to the diameter so that it directs the oncoming flow onto the semicircular cup. A comparison of the Vinh-Houmaire turbine with the Savonius is relevant here.

The Savonius suffers from certain disadvantages. It has to be supported from the top end and this results in a more expensive tower. However the most significant disadvantage is that the torque goes through wide variation when plotted against wind angle. Twice in a cycle (0 to 360^0) it actually becomes slightly negative (Le Gourieres,1982). The Vinh-Houmaire turbine is likely to have a more uniform torque because of its geometry; however, its torque characteristics have not been reported by the inventors. Also one can put a strong vertical torque tube through the center of the turbine without affecting its performance and hence it need not be supported from the top end (This advantage has not been reported by the inventors (Le Gourieres,1982)). This results in less expensive tower. The power coefficient

of the Vinh-Houmaire turbine is given against tip speed ratio by Le Gourieres(1982). The torque data is not given. The thrust (drag) and side (lift) force data which are necessary for tower design are also not available in literature. Hence the present experiments have been carried out to measure drag, side force and torque and verify the performance in a wind tunnel which has a test section size of 3 m $\times$2.25 m. The turbulence level and flow angularity of the wind tunnel are $< 0.1\%$ and $< 0.2^0$ respectively. Maximum Reynolds number based on diameter achieved is 8.87×10^5.

Chapter 2

EXPERIMENTS

2.1 INTRODUCTION

As the theoretical and computational analysis is difficult with Vinh-Houmaire turbine, wind tunnel experiments are used in this thesis to evaluate its performance. Experiments are carried out in the National Wind Tunnel Facility (NWTF). The rotor model was prepared previously for static testing but all other important parts for mounting the model inside the wind tunnel and measuring power are fabricated.

2.2 MODEL FABRICATION

The Vinh-Houmaire rotor shown in figure 5 consists of two top and bottom plates, three pairs of semicircle and flat plate. These are arranged in a particular configuration (figure 6) which shows a horizontal cross section of the model. The three pairs are fitted in between two horizontal circular end plates. This rotor was fabricated previously for stationary testing. The model parameters are as follows,

- Diameter of rotor = 700 mm
- Height of rotor = 500 mm
- Projected area = 0.35 m^2
- Diameter of semicircle = 233 mm
- Height of the flat plate = 500 mm
- Width of the flat plate = 280 mm
- Thickness of the flat plate = 3 mm

The following are the major components of the turbine that are fabricated for dynamic testing of this rotor.

2.2.1 SHAFT

Shaft is made up of cold drawn bright mild steel rod. As the shaft length (670 mm) is excessive for machining on lathe hence we have chosen cold drawn bright mild steel rod to avoid any sort of misalignment due to machining. The diameter of this shaft is 16 mm (Refer Figure 7). An indent of 6 mm diameter and 2 mm deep as shown in the figure is provided for fixing the lower flange on the shaft with help of grub screws. Tap of M6 is provided on top of shaft for fixing the upper flange with the help of bolt. Lower part of shaft is having step of 12 mm on which bearing of ID 12 mm is fixed and step of 11 mm is provided for assembling and dismentling of bearing.

2.2.2 Lower and upper bearing housing

Lower bearing housing is made up of mild still material. The long shaft is supported at its lower end by two bearings which are placed inside bearing housing (See figure 8). Two SKF ball bearings of inner diameter ϕ 12 mm and outer diameter of ϕ 32 mm are selected. To avoid any misplacement of bearings the steps are provided.

Upper bearing housing provides support to the shaft at its upper end to reduce its overhang. We have selected SKF ball bearings with inner diameter of ϕ 30 mm and outer diameter ϕ 62 mm. This bearing is placed on the boss of upper flange and held in position by the bearing housing with its inner diameter ϕ 62 mm and outer diameter ϕ 90 mm. To keep the bearing in fixed position the cap is provided on its top while spacer is provided on bottom. The cap is bolted with the bearing housing by using M6 holes which are 90^0 apart and on PCD of ϕ 80 mm. (Refer Figure 9)

2.2.3 Front end adaptor

It is the important component (shown in figure 10) as it enables model assembly to mount on balance. But the total weight that the balance can support is restricted by the allowable vertical load limit of the balance.The specified load limit for the available balance is 25 kgs. Hence to reduce the total weight of system, front end adaptor is made up of aluminium. It's outer diameter is 95 mm and height is 232.5 mm. The top portion is provided with cavity to accommodate lower bearing housing. While bottom portion is provided with tapered cavity to accommodate balance. The balance and adaptor is kept in fixed position by the use of rectangular key.

2.2.4 Upper and lower flange

These are made up of aluminium to reduce the total weight of the model. Both the upper and lower flange are shown in figure 11 and 12 respectively. Outer diameter of the upper flange is ϕ 100 mm while diameter of boss is ϕ 32 mm. A through hole of 16 mm is provided for shaft to pass through the upper flange. 4 holes of M4 which are 90^0 apart are provided on PCD of ϕ 80 mm for fixing this flange with the top surface of model with the help of bolts.

Lower flange outer diameter is ϕ 200 mm while diameter of boss is ϕ 50 mm. A through hole of 16 mm is provided for shaft to pass through the flange. 3 holes of M4 which are 120^0 apart are provided on PCD of ϕ 60 mm for fixing the flange with the bottom surface of model with help of bolts.

2.2.5 Brake shoe arrangement

The brake shoe arrangement for torque measurement can be seen in figure 13. Brake shoes are fixed on one end of M4 bolts and these bolts are bolted on 12 mm M. S. rod. There are two rods with 3 brake shoes on each (In figure only one of the rod is shown). These rods are provided with threading of M10 on its ends. These rods are fixed on the brake rod holding disc by using this threading. Brake rod holding disc is made up of mild steel with outer diameter ϕ 80 mm and inner diameter of ϕ 40 mm. This disc is inserted on the outer periphery of lower bearing housing and fixed in certain position by using grub screws.

The brake shoe arrangement consists of two steel rods on which 6 rubber pieces have been mounted to apply braking torque. We stitched four rubber packings on each of this brake shoes for providing spring effect such that contact is maintained with bottom surface

of model. When a brake force is applied on bottom surface of model the torque is being transmitted to balance and balance read it as moment. The rubbers are located at different radii thus varying the moment arm. This variation of moment arm is helpful in varying torque to be read by the balance.

2.3 EXPERIMENTAL SET UP

The purpose of this experiment is to measure the forces and torque generated on a scaled model of wind turbine at different operating condition. The model consists of 3 pairs of flat plate-semicircle, bounded by a circular top plate and bottom plate. The model diameter and height are 0.7 m and 0.5 m. The complete model mounted in wind tunnel as shown in figure 14.

Initial experiments were carried out in the wind tunnel with a model supported at the bottom. The top bearing was not present in these experiments. But the model vibrations could not be arrested at high speeds and low tip speed ratio. To overcome this problem we came up with some modifications in set up (See Figure 15). We supported the shaft by bearing at its top end. the bearing is placed inside bearing housing. The bearing housing is fixed by using 4 tension wires inside test section (Refer Figure 16). Turn buckles are used to adjust the tensions. The wires are hung to the hooks available on the walls of test section. The tension wires were making approximately 10^0 angle to the horizontal which helped in supporting the axial load exerted by model assembly on the balance. This arrangement worked very nicely and hence we could able to test the turbine at higher wind speed and low tip speed ratio i.e at larger rpm.

2.4 WIND TUNNEL SPECIFICATION

The testing of modified Savonius rotor is carried out in National wind tunnel facility (NWTF). The specification of wind tunnel used is given below,

- Return circuit, Continuous, closed jet and atmospheric .
- Interchangeable test section. .
- cross section : $3m \times 2.25m$.
- length : 5. 75 m (Upstream) + 3 m (Downstream) .
- Contraction ratio : 9:1 .
- Maximum wind speed : 80 m/s .
- Reynolds number : 5×10^6/m .
- Guide vanes : Simple circular type. .
- Honeycomb : Hexagonal .
- Antiturbulance screens : 4 .
- Turbulence level: $\leq 0.1\%$.
- Flow angularity: $\leq 0.2^0$.
- Fan : 4.64 m diameter, 12 bladed.
- Motor rating: 1000 kw, variable speed DC motor, 450 rpm

2.4.1 Balance specification and calibration

A simple calibration rig is used for checking and updating calibration matrix for NWTF force balances. Loading of one component at a time is done during calibration and load is applied in gravity direction. The balance calibration procedure is standardized, optimized and automated (except loading) for faster calibration. The load prediction capability is found to be within 0.25% of applied load as specified by manufacturer.

To calibrate the balance accordingly the balance is connected to calibration rig with it's sting end and a stiff loading sleeve is connected to model end of balance. Loads are generated by hanging dead weights attached to loading sleeve at an appropriate distance to axis. Lateral loads (side force, yawing moment)are generated after turning the balance through 90^0 around it's axis.

The load ranges of balance available in NWTF is as listed below;

	Balance A(Low range)			Balance B(High range)		
	Load range	Output in mv/v	Output in mv/5v	Load range	Output in mv/v	Output in mv/5v
Axial force (A_x)	25 kg	1. 637 mv at 25 kg	8. 19	120 kg	0. 683 mv at 100 kg	4. 10
Normal force-1 (N_1)	120 kg	0. 441 mv at 50 kg	5. 29	600 kg	0. 519 mv at 300 kg	5. 19
Normal force-2 (N_2)	120 kg	0. 431 mv at 50 kg	5. 17	600 kg	0. 528 mv at 300 kg	5. 28
Side force-1 (S_1)	35 kg	0. 398 mv at 25 kg	2. 79	150 kg	0. 956 mv at 150 kg	4. 78
Side force-2 (S_2)	35 kg	0. 397 mv at 25 kg	2. 78	150 kg	0. 981 mv at 150 kg	4. 91
Rolling Moment (R_m)	13 kg-m	0. 916 mv at 10 kg-m	5. 95	120 kg-m	0. 651 mv at 80 kg-m	4. 88

From past experience and as per our prediction the torque and other forces are well within limit for lower range balance hence lower range balance (balance A) is selected for the experiments.

Analysis is done using slope method. In this method for each data set the 6 signals obtained from the balance are plotted against applied load and straight line fits are obtained. For example, if load applied is N component then each of 6 signal components A_x, N_1, N_2, S_1, S_2 and Rm are plotted against the applied load N_1 and the six straight line fits are obtained by least square technique. This procedure is repeated for six data sets to obtain

36 components C_{ij} as shown in following equation,

$$S_i = \sum_{i=1}^{6} C_{ij} \times L_j$$

These coefficients C_{ij} form the elements of the coefficient matrix. When a load matrix Li (a 6×1 column matrix) is premultiplied by 6×6 coefficient matrix the result is signal matrix. The coefficient matrix is inverted to obtain inverse matrix. When inverse matrix is premultiplied to the signal matrix, the result is load matrix.

$$L_i = \sum_{i=1}^{6} {C_{ij}}^{-1} \times S_j$$

Force and torque measurements were carried out using 6 component strain gauge balance. Since is balance is mounted under the model itself it gives the predicted loads in body axis system. So to get aerodynamic loads in wind axis system the detailed data reduction routine was followed which is given below, Forces and moments at balance center:

$$A_{x_{bal}} = A_x$$

$$N_{bal} = (N_1 + N_2)$$

$$S_{bal} = (S_1 + S_2)$$

$$M_{p_{bal}} = (N_1 - N_2) \times 0.065$$

$$M_{y_{bal}} = (S_1 - S_2) \times 0.065$$

$$M_{r_{bal}} = R_m$$

The normal force and side force measurement gauges are fixed symmetrical to center at distance of 0.065 m. That's why while calculating pitching and yawing moment the difference in normal channels and side channels is multiplied by 0.065 m respectively. But in experiment we haven't gave any pitching or yawing moment to the model. We were only interested in the Rolling moment i.e the braking torque.

2.4.2 Measurement of speed of rotation

We used photo tachometer for measuring the rpm of turbine as we have to measure it from outside the test section. We pasted an adhesive reflective tape on turbine model and projected the visible light beam exactly on the target i. e. reflective tape through the glass window of test section. The specifications of photo tachometer used are,

- Test range : 2. 5 to 99999 rpm.
- Resolution : 0. 1 rpm (2.5 to 99999 rpm)

  1 rpm (over 1000 rpm)

2.5 Wind tunnel tests (dynamic tests)

Unlike previous experiment (Satyakan,2002) we have carried out dynamic testing if the rotor. In (Satyakan,2002) the turbine performance was tested statically. In the present experiment we allow the turbine to rotate freely or under some braking.

For the first time an aerodynamic balance is used for measuring wind turbine power. All the previous measurements are carried out using generators or air motor and load cell combination. Brakes were applied as discussed in section 2.2.5 and the braking torque was measured.

Model was mounted on the balance inside test section of the wind tunnel. We recorded the torque produced by turbine at different braking condition and at different free stream velocities. Side force signal from balance was recorded so that we could measure the rpm of turbine as well as to keep watch on vibrations of model. Non contact tachometer was also used to record the rpm of turbine. Following steps were followed to take the readings,

1. Record no wind data.

2. Increase the tunnel velocity to 4 m/s. The model will start rotating. At this velocity record the data through data acquisition software provided by NWTF. At the same time record the revolutions of the turbine manually using non contact digital tachometer.

3. Move inside the test section when tunnel is on and apply the brakes manually. Come outside the test section and close the tunnel door.

4. Due to brakes the rpm of turbine will go down hence note down a new reading of revolutions and acquire the data through software.

5. Increase the wind velocity in step of 2 m/s each time and record the data and rpm measurement. In short record the data at 6 m/s, 8 m/s , 10 m/s. . . .. upto 20 m/s.

6. Again decrease the wind velocity in step of 2 m/s each time and record the data through data acquisition software and record rpm measurement. In short record the data at 20 m/s, 18 m/s , 16 m/s. . . . . upto 4 m/s.

7. Then stop the tunnel and record the no wind data.

8. Repeat the same procedure but start the experiment from some higher wind velocity say 6 m/s instead of 4 m/s so that we can apply somewhat higher friction through brakes.

9. Now start the experiment at say 8 m/s and repeat the procedure at some different braking condition.

10. We can't enter into wind tunnel beyond 8 m/s hence to vary the friction at 4 m/s, 6 m/s, 8 m/s use more number of brakes (Total 6 brake shoes provided).

A typical balance output is shown in figure 17. We can see the various controls on this front panel. The acquired voltage signal is plotted on the waveform graph as shown in figure. The plot menu is provided to select the force or moments like axial force, side force, drag etc.for plotting on a waveform chart. We can see the tunnel velocity in the indicator provided. The controls like data set, scan rate are also provided. Figure shows the plot of side force.

2.6 WIND TURBINE FIELD UNIT

A wind turbine field unit had been erected near the Airstrip before I joined the Department as a student. This was a part of an ARDB supported project. The field unit had the following features :

The wind turbine field unit had a tower, table and flexible steel rope for transmission of power. It used sprocket and chain mechanism of bicycle to rotate a dynamo using mechanical power from wind turbine. But there was some history of troubles with the power transmission. The cycle frame was in horizontal position and hence there was slack in chain resulting in frequent dislodgement of the chain out of sprocket and stoppage of power transmission. Then sprocket, free wheel and chain mechanism was replaced with belt drive but the cycle frame was retained. There was some misalignment in the planes of pulleys and the belt tension was also large. It did not perform satisfactorily.

I contributed in finding a remedy for above problem. To overcome the power transmission problem, we removed the cycle frame completely from our design. We made the arrangement

of pulley drive (diameter ratio 1:2) in which bigger pulley is located exactly on the axis of wind turbine rotor. Schematic diagram of this arrangement is as shown in figure 18. The power is transmitted from the wind turbine to bigger pulley as in the previous arrangement, that is, through wire and turnbuckle. This power is transmitted to smaller pulley through belt. The cycle wheel is fixed on the shaft of smaller pulley in the horizontal plane (See Figure 19 for plan view). In this design, we have made,

- An arrangement for adjusting the tension of belt. (See Figure 20)
- Alignment of planes of pulleys.

2.6.1 FABRICATION

The following components were fabricated for satisfying the design needs.

(1)BEARING BLOCK-1 AND BEARING BLOCK-2

These are made up of C. I. blocks of 100 mm × 50 mm ×50 mm. Shaft-1 is supported in the block-1 by two SKF bearings of OD ϕ32 and ID ϕ12.See figure 21. Shaft-2 is supported in the block-2 by two SKF bearings of OD ϕ36 and ID ϕ 15 See figure 22. To maintain the two bearings in perfect alignment the blocks are bored in one go. A sleeve is inserted in between two bearings to provide location. The bearing block-1 is mounted on machined angle iron slides with help of M6 bolts. But the bearing block-2 is not fixed on the iron angle as it is provided with one degree of freedom to adjust the distance between two blocks.

(2) SHAFT-1 AND SHAFT-2

These are made up of EN-8 material. Shaft-1 is inserted in bearing block-1 which is right underneath of turbine. It is provided with M16 threading on its upper end as shown in figure 23. Turn buckle's lower end is fixed on this threading while upper end of turn buckle is fixed with cable coming from turbine. Bigger pulley is fixed on lower end of shaft-1 exactly underneath of bearing block-1. Thus power is transmitted from turbine to bigger pulley through shaft-1 and turn buckle arrangement.

Shaft-2 is inserted in bearing block-2. The smaller pulley is fixed on lower end of shaft-2 exactly underneath of bearing block-2 (See figure 24). Power is transmitted from bigger pulley to smaller pulley through the belt drive. The diameter of shaft at its upper end is exactly made equal to inner diameter of axle of cycle wheel. The cycle wheel is press fitted on the upper end of shaft.

The rear fork of a bicycle is suitably mounted on rectangular iron frame at bottom of field unit. The fork supports the dynamo (cycle dynamo of specification 6 volts and 5 watts) which engages on rubber tyre of cycle wheel. Figure 25 shows the field unit and figure 26 shows the bottom part (with cycle wheel) magnified.

We demonstrated the transmission of mechanical power to cycle wheel successfully. But we were unable to conduct any experiment on the field unit due to shortage of time.

Chapter 3

RESULTS AND DISCUSSIONS

3.1 RESULTS OF DYNAMIC TESTING

The axial force (constant weight of the model and tare), side force, drag force and rolling moment are recorded using the wind tunnel balance. Data has been acquired using Lab-VIEW software and NI (PCI-6034) DAQ card. Readings from the experiments, which were basically voltage signals, were reduced to forces and moment using the calibration coefficient as discussed in chapter 2. Tunnel speed is measured using a pitot tube which is placed at the entry of the test section.

The dynamic testing of the Vinh - Houmaire turbine is carried out in two rounds of experiment. In the first round the rotor was suppported only from the bottom with sting and balance. There are no other external supports here. Therefore the side force and drag force readings are meaningful. From this data we have calculated the coefficient of drag C_D and coefficient of lift C_L. The C_L and C_D are plotted against λ as shown in figure 26(A) and 26(B) respectively. The magnitude of C_L is increased in negative direction as the λ goes

on increasing. C_L is negative as the direction of lift force generated due to Robin-Magnus effect is negative(see figure 6 for defination of forces acting on 6 component strain gauge balance). If we assume the turbine to be a solid cylinder, rotating in anticlockwise direction in a moving flow from left to right when looking from top, it will give a downward force as per the magnus effect and the value of the side force will go on increasing as the rpm of turbine increases. The C_D value is low at low value of λ and reaches its maximum value at λ of 0.4 then again the value of C_D goes down. This nature of curve is similar in case of C_P Vs λ curve (figure 30). This is expected as power is nothing but drag times velocity hence we can relate C_P and C_D directly.

Mean value of C_D and C_L comes out to be 1.2697 and -0.2624 respectively. The C_D and C_L are calculated as follows,

$$C_D = \frac{D}{1/2 \times \rho \times A \times V^2}$$
$$C_L = \frac{L}{1/2 \times \rho \times A \times V^2}$$

where,

D= drag force in N

L= Lift (side) force in N

A= Projected area of turbine= 0.7 m $\times$ 0.5 m.

V= Freestream velocity in m/s.

For the forces direction acting on model see figure 6. This results are tabulated in table no. 1 and 2.

Figure 27 shows the different forces and moments measured in terms of voltage for tunnel speed of 6 m/s when turbine was rotating without any brake loading. The rpm and tip

speed ratio for this case is 135 and 0.8 respectively. Figure 28 shows the different forces and moments measured in terms of voltage for the same tunnel speed i.e. 6 m/s when turbine was rotating with the brake load applied. The rpm and tip speed ratio for this case is 30 and 0.18 respectively. It can be observed from these figures that drag (normal force) and lift (side force) is oscillating consistently due to three pairs of semicircle - flat plate combination.

The coefficient of torque(C_Q) and coefficient of power (C_P) are plotted against tip speed ratio (See figure 29 and figure 30). The maximum value of C_P is 0.13 at a tip speed ratio of 0.37 and maximum value of C_Q is 0.51 at a tip speed ratio between 0 to 0.15. But we could not conduct the experiment at higher wind speeds as model started vibrating as it was not supported at the top by stay wires. The brake shoe arrangement also did not work properly. We got the negative torque for some data points which is impossible hence the accuracy of the results for this experiment was doubtful. Hence we decided to modify the experimental set up and brake shoe arrangement and conducted the second round of experiment. The changes made are described in previous chapter.

For the second round of experiment the model is supported at its top by the bearing and the bearing is held in position with help of tension wire and turn buckle arrangement, that's why the side force and drag is not having any meaning as this forces are absorbed by the tension wires. However these forces are meaningful to judge the tension in the stay wires Figure 31 shows the different forces and moments measured for the second round of experiment when the turbine was rotating freely. The tunnel speed for this case is 8 m/s. The rpm and tip speed ratio for this case is 170 and 0.75 respectively. It can be observed from this figure that the measured torque in voltage is near zero for this case and drag (normal force) and lift (side force) are oscillating consistently due to three pairs of semicircle

- flat plate combination.

Figure 32 shows the measured values of forces and moments for the same wind speed i.e. 8 m/s but with brakes applied and thus the rpm of the turbine is lower. In this case rpm is reduced as the brake is applied. Corresponding tip speed ratio and rpm is 0.34 and 76 respectively. Once again the consistent oscillations of normal and side force are seen in figure 32.

The figure 33 shows power spectrum of drag. This measures the frequency of oscillations and hence the rpm of turbine rotor. In this case the peak occurs at 2.5 Hz which means rpm is 150. The rpm is also measured independently using a rpm meter and manually using a stop watch for verification.

Figure 34 shows the torque (in terms of voltage) vs time during a complete rotation. For any angle of attack there are atleast two plates of the turbine which gives positive torque and only one gives negative torque. Hence this is unidirectional and at no point it produces the negative torque as in case of Savonius. The flat plate directs the air flow towards the cup which adds to the drag. Whereas the flat plate acts like a splitter plate which reduces the drag by narrowing the wake when moving upwind. Hence, net drag difference gives a large torque.

Figure 35 shows the variation of side force with respect to turbine rotation in degrees. The plot shows the side force in voltage for five cycles of rotation at freestream velocity of 8 m/s when the turbine is freely rotating. The turbine is rotating at 170 rpm. Figure 36 shows the variation of side force with respect to turbine rotation in degrees. The plot shows the side force in voltage for five cycles of rotation at freestream velocity of 8 m/s when the brake force is applied on the turbine. The turbine is rotating at 75 rpm. The above two plots are

important while experimenting for observing the behaviour of turbine. The model is kept in position by adjusting the tension in tension wires as discussed in previous chapter. This plot is indication that the model is in good alignment with the balance axis and tension in all the stay wires are of same order and no wire is becoming slack during a cycle. This can be judged from the regular behaviour without a spike in the cyclic side force. The model is supported at its top by the bearing and the bearing is held in position with help of tension wire and turn buckle arrangement, that's why the side force and drag is not having any meaning as this forces are absorbed by the tension wires.

Variation of dimensional torque for different rpm for the different wind speeds are shown in figure 37. It can be observed that the starting torque for this rotor is high and goes to zero as rpm of turbine increases. Thus it provides automatic power control; hence there is no need of providing storm security devices which is an important part of horizontal axis wind turbine.

Variation of dimensional power for different rpm for the different wind speeds are shown in figure 38. It can be observed that power shows increasing trend from lower rpm to certain rpm, reaches peak and then goes down to zero at higher rpm. This again proves that this rotor does not need any storm security device which enables this rotor to cope with higher wind speeds automatically. Power is calculated as,

$$P = \frac{2 \times \pi \times N \times T}{60}$$

Where,

P = Power in watts

N = rpm of model

T = Torque in N-m

The nondimensional torque variation for the 2nd round of experiment is shown in figure 39 and figure 40. The nondimensional power variation for the 2nd round of experiment is shown in figure 41 and figure 42.

Nondimensional torque, known as torque coefficient(C_Q) is calculated as,

$$C_Q = \frac{\text{Torque in N-m}}{1/2 \times \rho \times A \times V^2 \times R}$$

where

$$\rho = \text{ Density of air } = 1.225 \text{ kg}/m^3$$

$$A = \text{ Projected area of model } = 0.5m \times 0.7m$$

$$R = \text{ Radius of model } = 0.35m$$

Tip speed ratio is defined as ratio of turbine tip speed $\omega \times R$ to wind speed V_∞

$$\lambda = \frac{\omega \times R}{V_\infty}$$

$$\lambda = \frac{2 \times \pi \times N \times R}{60 \times V_\infty}$$

where,

$$\lambda = \text{ Tip speed ratio,}$$

$$R = \text{ radius of model } = 0.35m,$$

$$V_\infty = \text{ Free stream velocity in m/sec.}$$

λ is the correct nondimensional abscissa for plotting for estimating the turbine performance. The Reynolds number varies in all the experiments are from 1.87×10^5 to 8.87×10^3.

Figure 39 shows the variation of torque coefficient (C_Q) with λ. The C_Q varies with λ in the range of λ= 0.15 to 0.7 for this turbine. The maximum value of C_Q is 0.42 at a λ of 0.15.

Figure 41 shows the variation of power coefficient (C_P) with λ. The maximum C_P is 0.11 at a λ of 0.36.

Vinh and Houmaire studied this rotor and claimed the maximum coefficient of power of about 0.3 for a tip speed ratio of 0.7. See figure 43 (Le Gourieres,1982). The present experiment shows value of C_P around 0.11 which is well below that claimed by Vinh and Houmaire.

The C_P and C_Q curves against tip speed ratio for two bucket and three bucket Savonius rotor are given in figure 44 and figure 45 respectively (Blackwell,1977). The power coefficient for two bucket Savonius rotor peaks near the tip speed ratio of 0.9. The peak value of power coefficient is about 0.24. The maximum torque coefficient which is around 0.42 occurs at a lower tip speed ratio, in the vicinity of 0.4. The present experiment shows the comparable value of C_Q around 0.4 at a tip speed ratio between 0 to 0.15.

On the other hand three bucket Savonius rotor shows the maximum C_P of 0.15 which peaks at tip speed ratio of 0.7. The maximum value of C_Q for three bucket Savonius rotor is 0.37 and occurs at a tip speed of 0.2. So performance of Vinh - Houmaire model is comparable to three bucket Savonius rotor.

All the results of present experiments are tabulated in the Appendix.

Chapter 4

CONCLUSION AND FUTURE WORK

We have successfully demonstrated the following technologies :

1. Wind tunnel balance and a friction device can be used for measuring power.Power is measured with the help of a device similar to a brake dynamometer.

2. The torque measurement in wind tunnel shows that there is no negative torque during the entire cycle of rotation.

3. Torque is more uniform over a cycle of rotation compared to a Savonius rotor.

4. The C_P curve shows a maxima at 0.11. This result seems to be well below that claimed by Vinh and Houmaire (Le Gourieres, 1982) which is 0.32 at a tip speed ratio of 0.7.

5. The C_Q curve shows a maxima of 0.42 which is comparable to the value of Savonius rotor.(Le Gourieres, 1982).

6. The performance of rotor is comparable to that of American multiblade type horizontal axis rotor which is very bulky and heavy in construction. Whereas the Vinh - Houmaire

rotor has a lower weight and material cost and less expensive tower. It has high torque, low speed and simple construction.

4.1 FUTURE WORK

1. More tests are required or suggested with both static configuration and dynamic configuration with improved braking arrangement for power measurement.

2. Modification of turbine is required for improving the coefficient of power. The flat plate can be replaced with the airfoil section which can induce a stronger component of lift to improve the differential drag. This modification can also contribute for directing the oncoming flow more evenly into the semicircular cups

Bibliography

[1] Blackwell, B., F., Robert, E. Sheldahl, Louis, V Feltz July 1977, "Wind Tunnel performance data for two and three bucket Savonius rotors", *Sandia Laboratories, New Mexico,* **SAND76-0131**

[2] Ghosh, Kunal, Jan 17 - 19, 2003, "Wind Tunnel And Open Air Tests of Vertical Axis Wind Turbine Model", *The Twenty Sixth National Renewable Energy Convention of Solar Energy Society of India and International Conference on New Millennium - Alternative Energy Solutions for sustainable development, Coimbatore,* **pp. 386-391.**

[3] Ghosh, Kunal, June 1-6, 2003, "Experiments on Vinh-Houmaire Wind Turbine", *17th Canadian Congress of Applied Mechanics (CANCAM-03), The University of Calgary, Alberta, Canada,* **pp. 386-391, Vol.-II.**

[4] Johar, Vinay, May 1999, "Test of low cost Guy wire supported Vertical axis wind turbine", *M. Tech thesis, Aerospace department,IIT Kanpur.*

[5] Johnson, G. L., 1985, "Wind Energy systems", *Prentice Hall, New Jersey.* **pp. 1-22.**

[6] Le Gourieres, D. L, 1982, "Wind Power plants theory and Design", *Pergamon press* **pp. 124-42.**

[7] Poddar, Kamal, May 27-31, 2002, "Report of short term course on Introduction to wind tunnel testing techniques".

[8] Rathakrishnan, E., Sept, 1999, "Effect of splitter plate on bluff body Drag", *AIAA Journal.*

[9] Satyakan, Manjith March, 2002, "Design,Fabrication and testing of model of Modified Savonious rotor wind turbine", *M. Tech thesis, Aerospace department,IIT Kanpur.*

FIGURES AND PHOTOGRAPHS

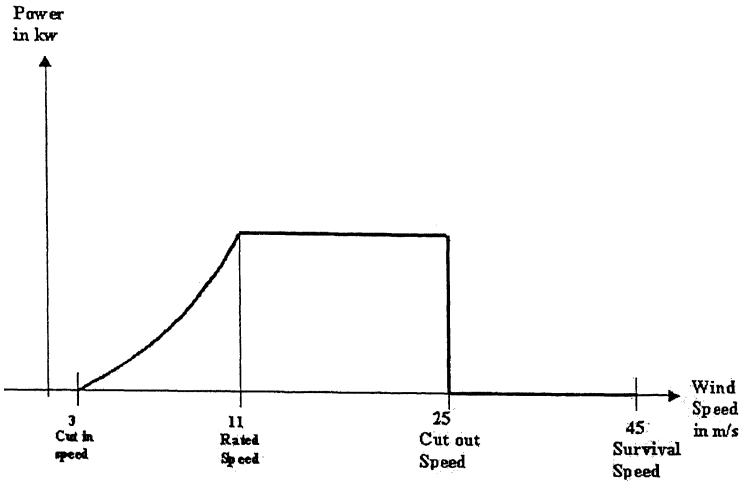

Figure 1: Power V/s wind speed curve.

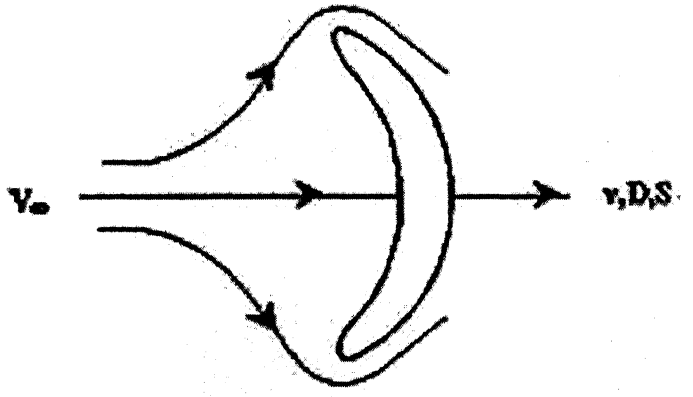

Figure 2: Drag translator.

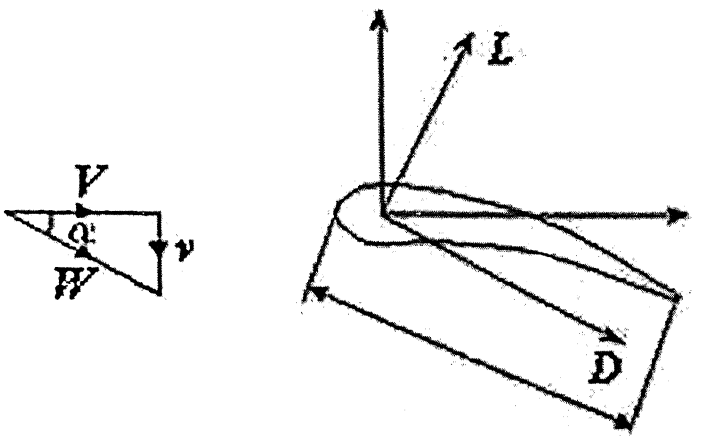

Figure 3: Lift translator.

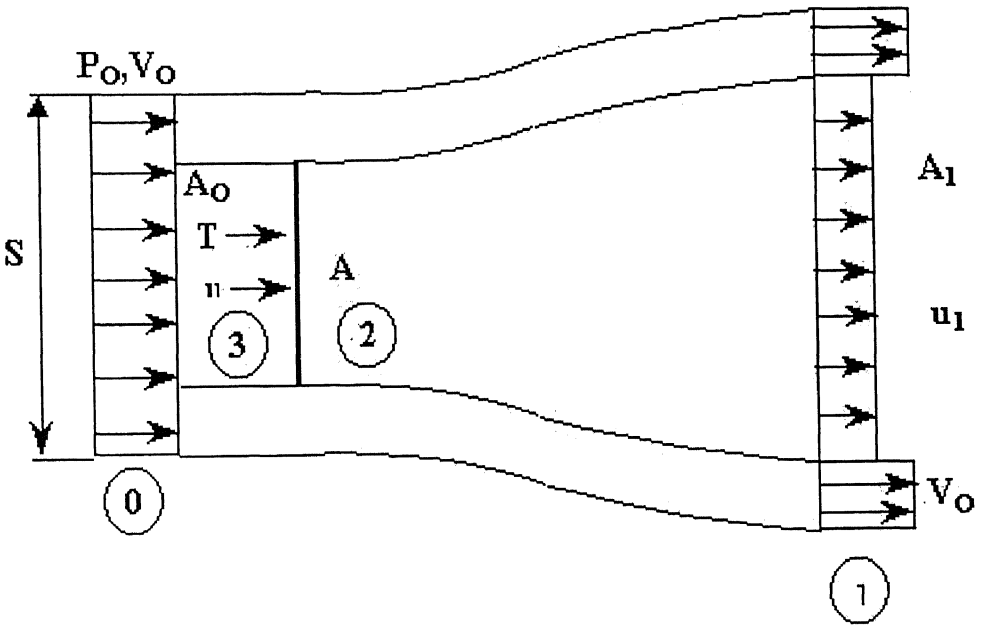

Figure 4: Rankine froude theory

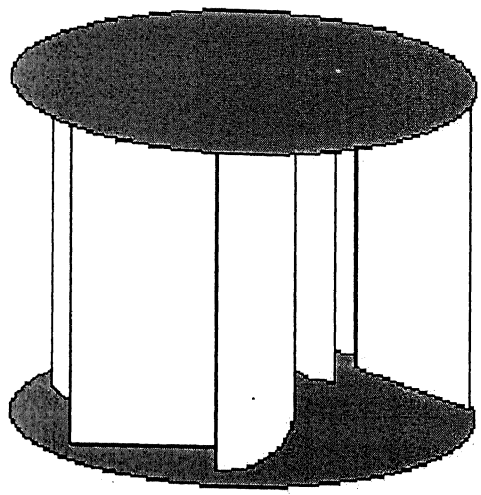

Figure 5: Vinh-Houmaire rotor

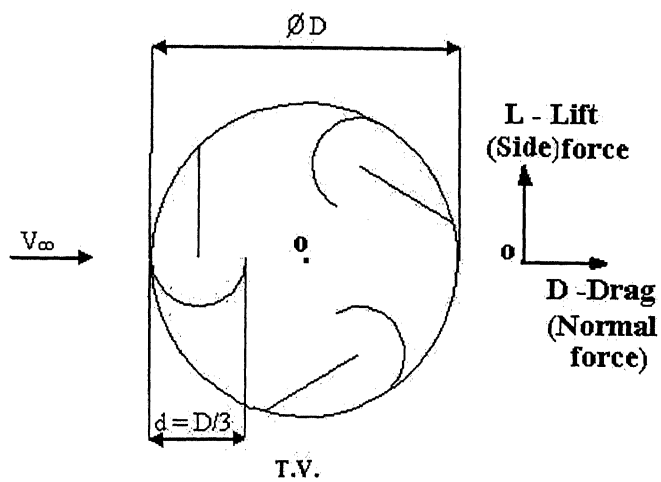

Figure 6: Cross sectional view of Vinh-Houmaire rotor

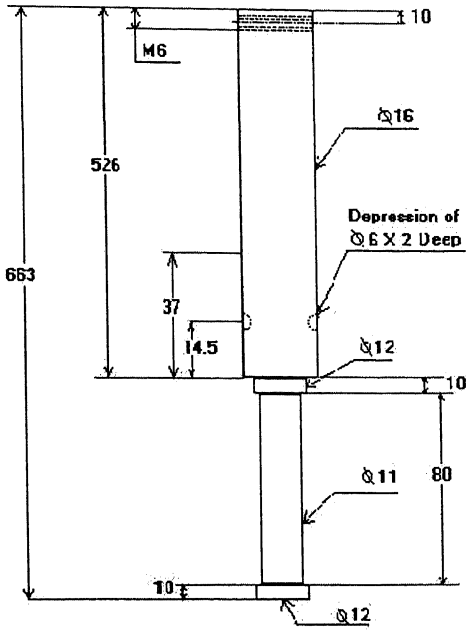

Figure 7: Shaft

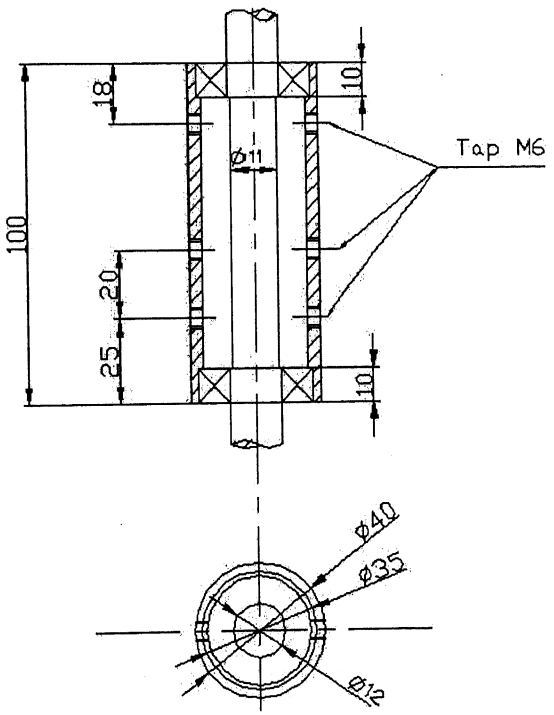

Figure 8: Lower bearing housing.

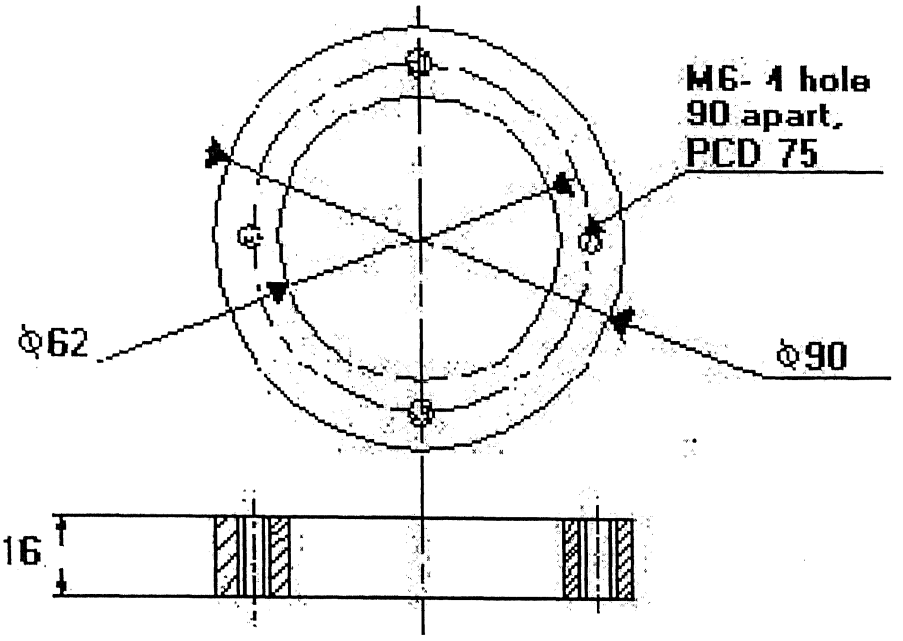

Figure 9: Upper bearing housing.

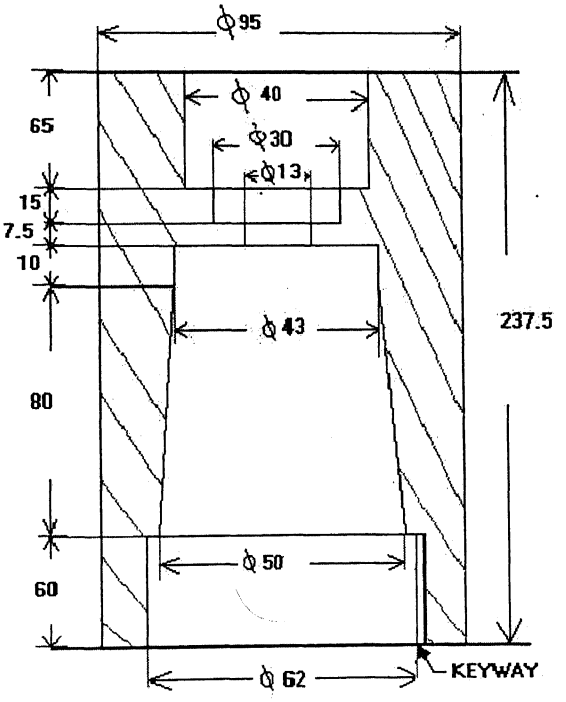

Figure 10: Front end adaptor.

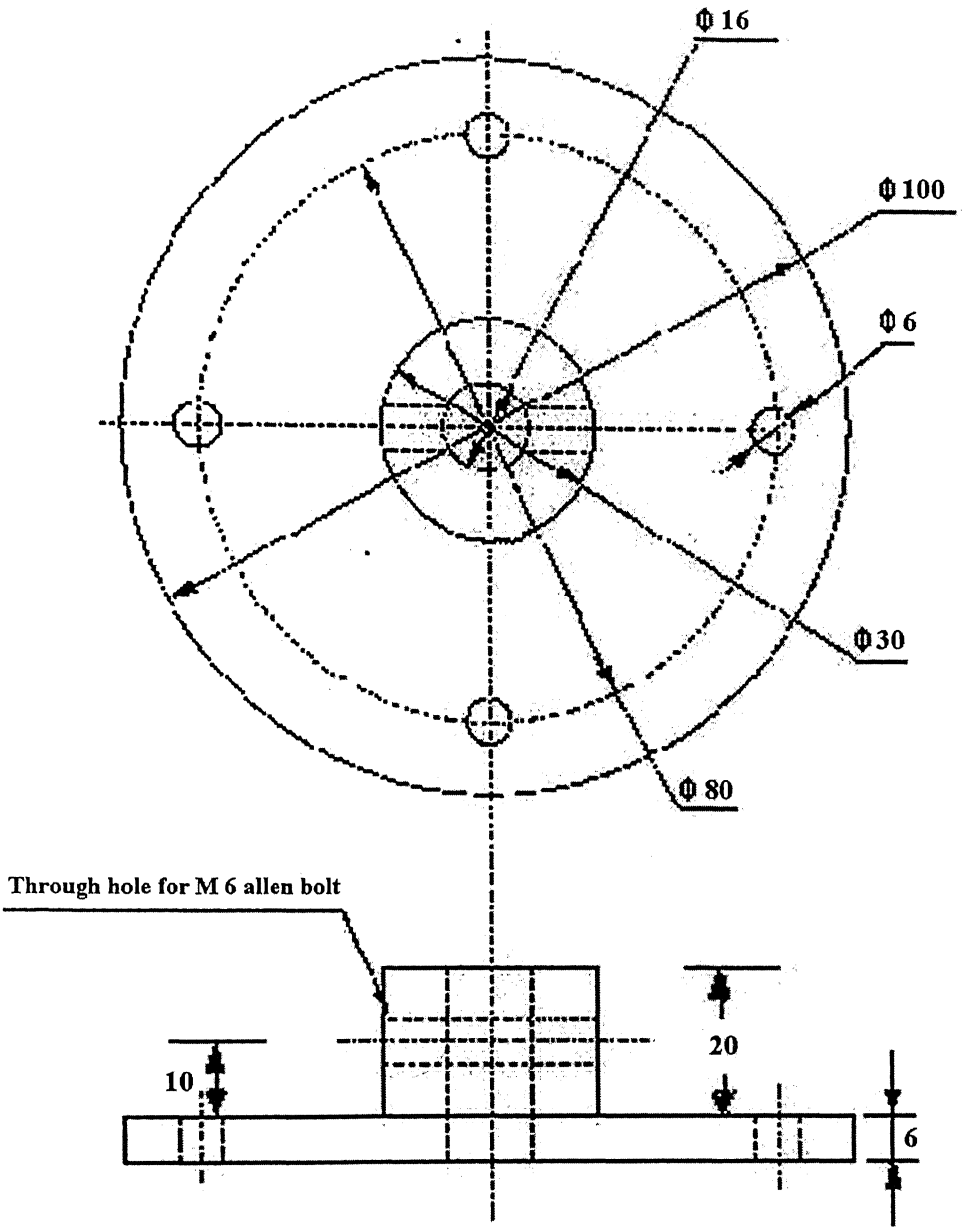

Figure 11: Upper flange.

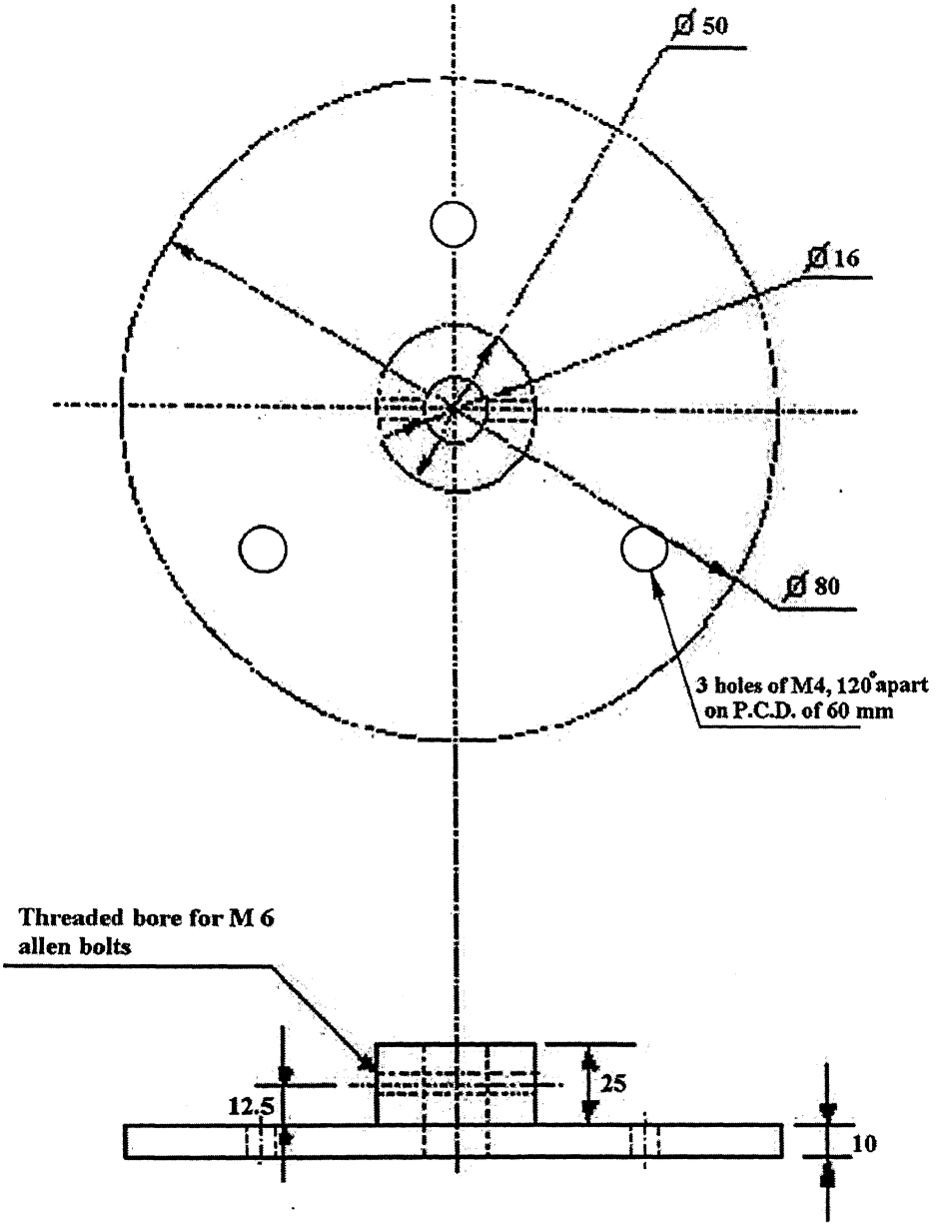

Figure 12: Lower flange.

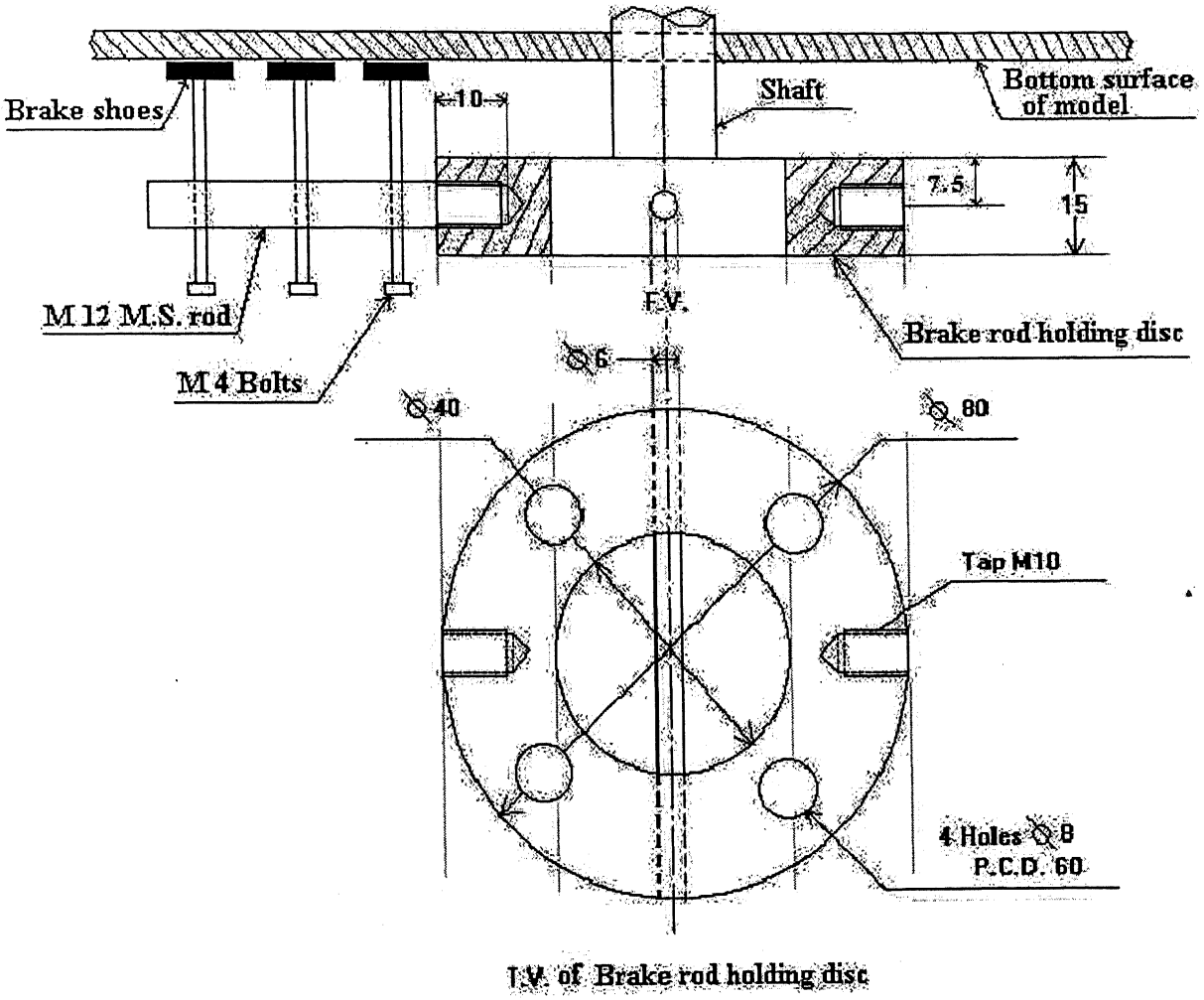

Figure 13: Brake shoe arrangement

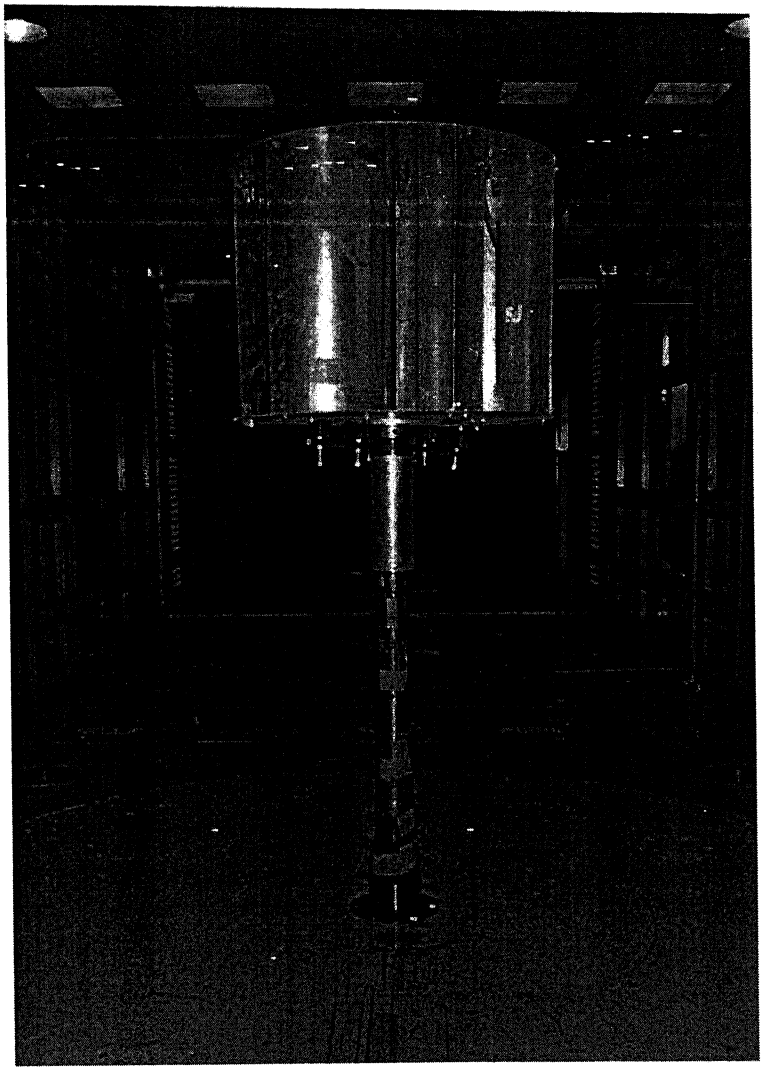

Figure 14: Photograph of model inside wind tunnel

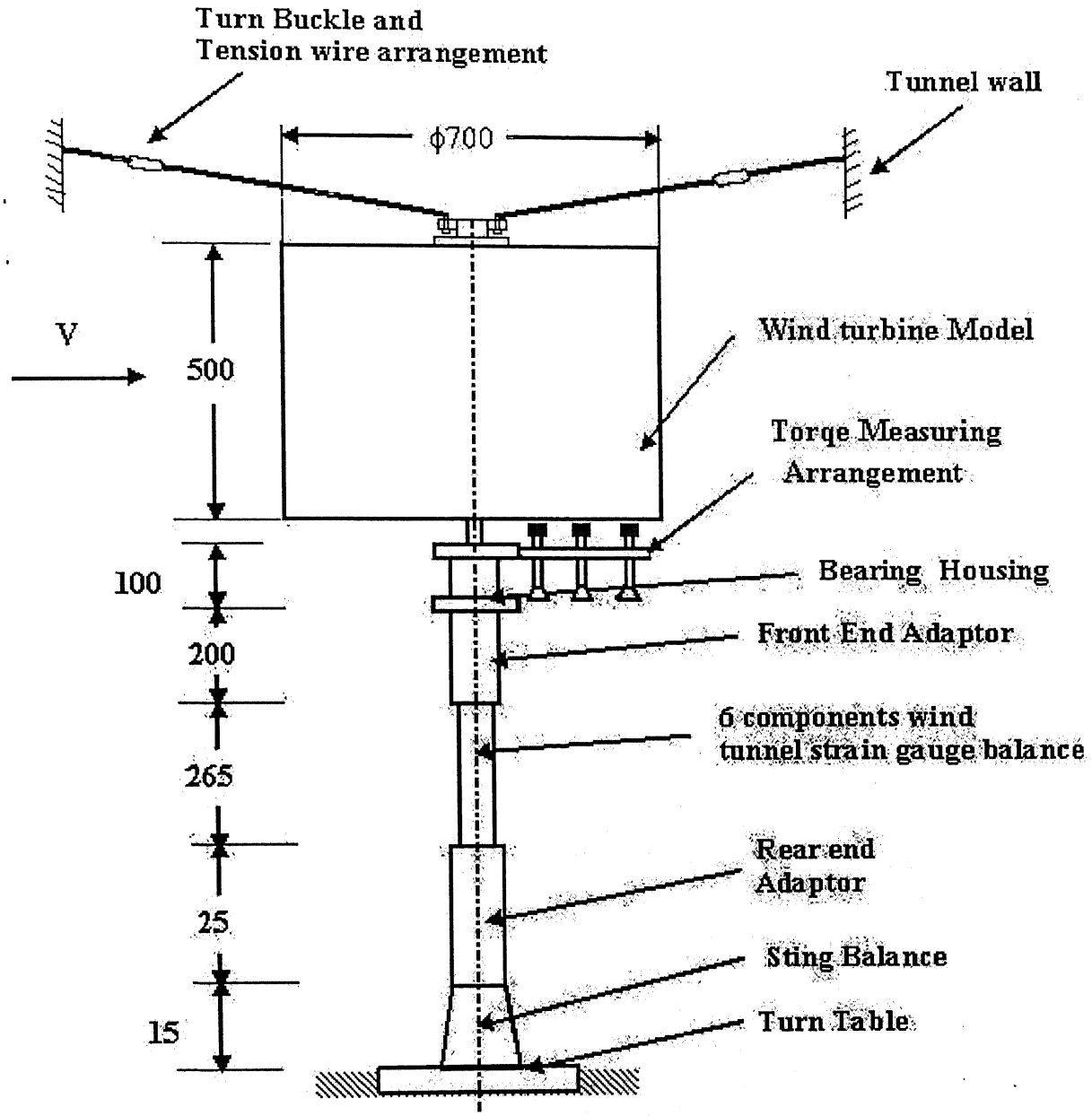

Figure 15: Schematic diagram of modified experimental set up

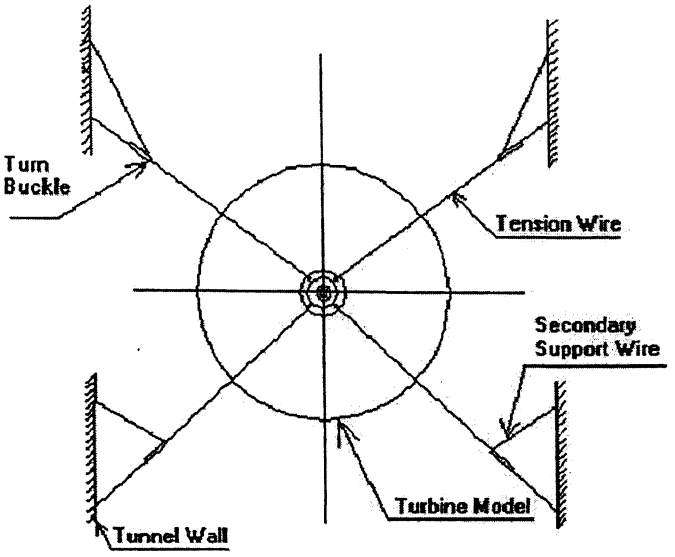

Figure 16: Tension Wire Arrangement.

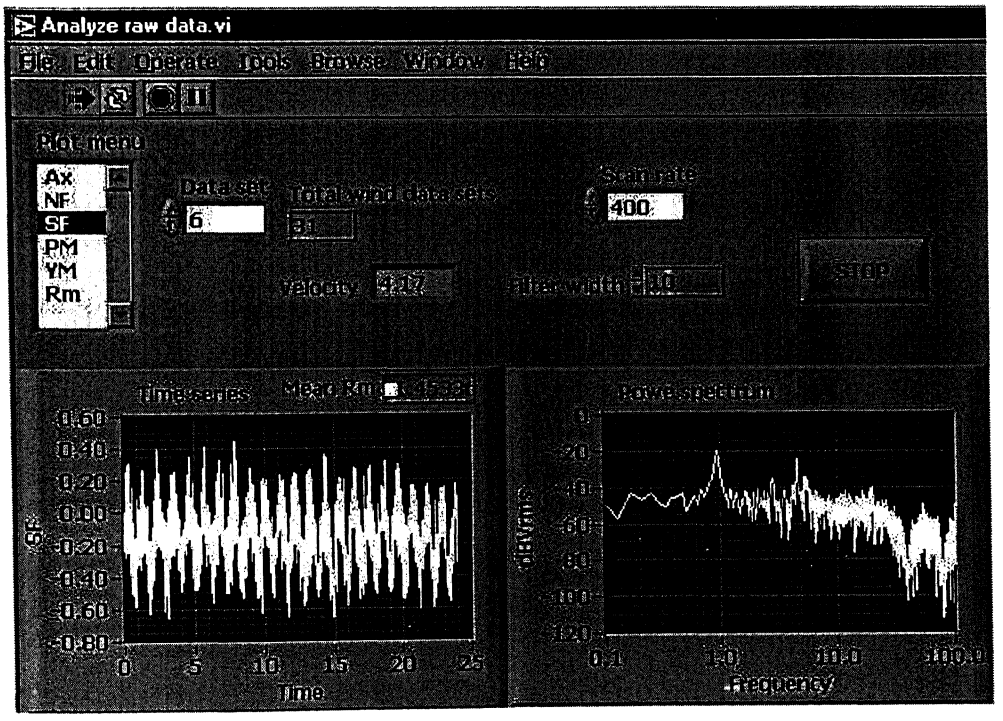

Figure 17: Typical LabVIEW output on front panel

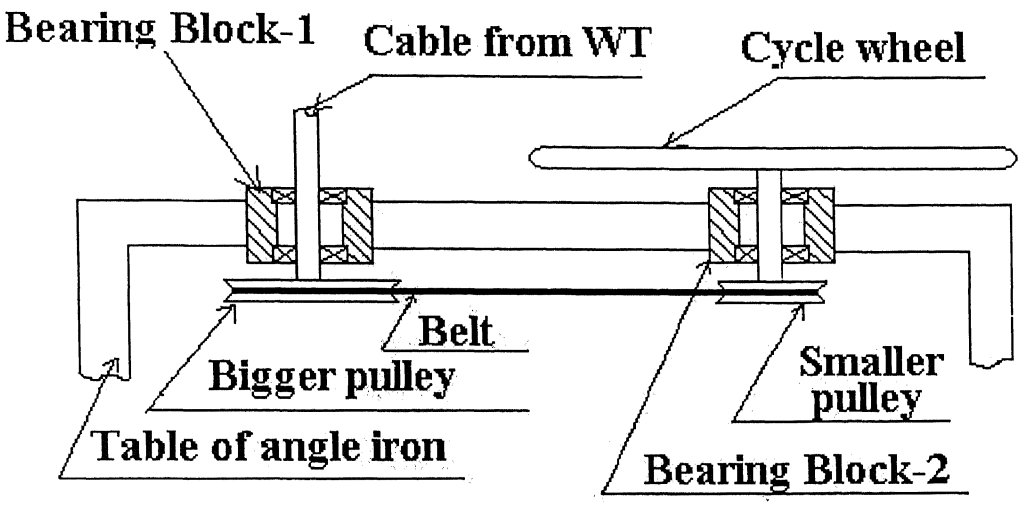

Figure 18: Bearing mounted pulleys and cycle wheel

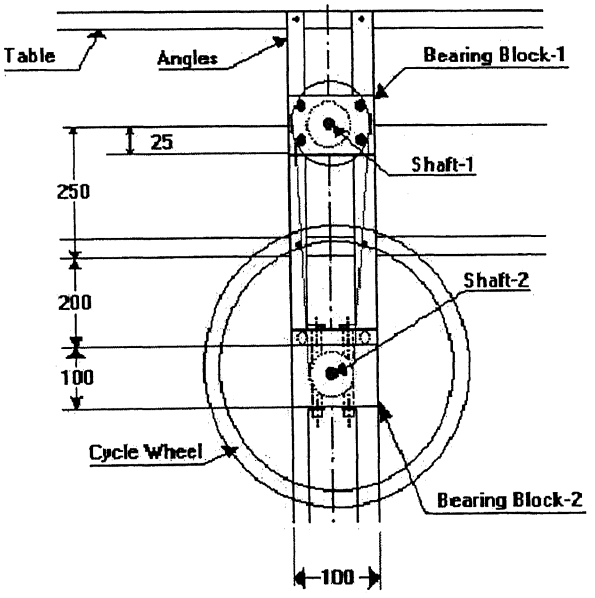

Figure 19: Schematic of power transmission system of field unit.

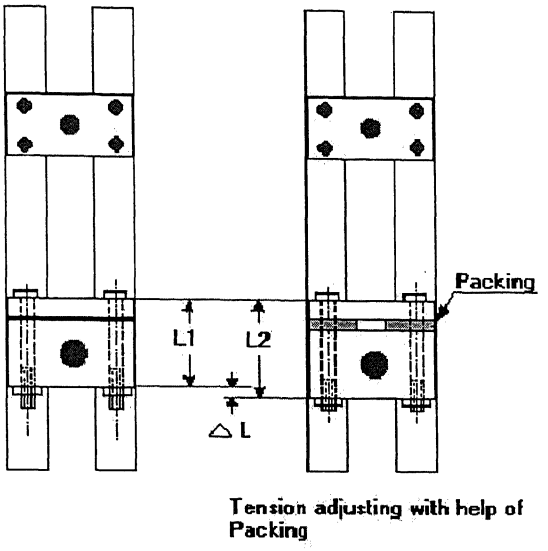

Figure 20: Tension adjustment.

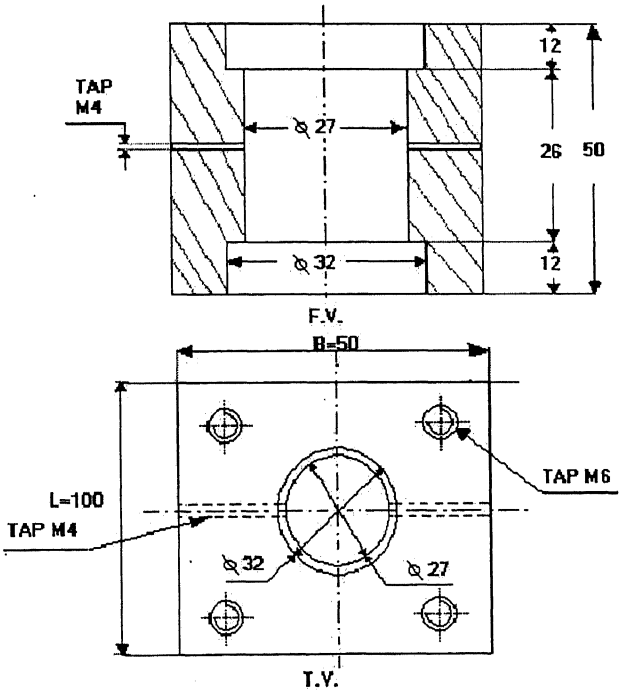

Figure 21: Bearing block - 1.

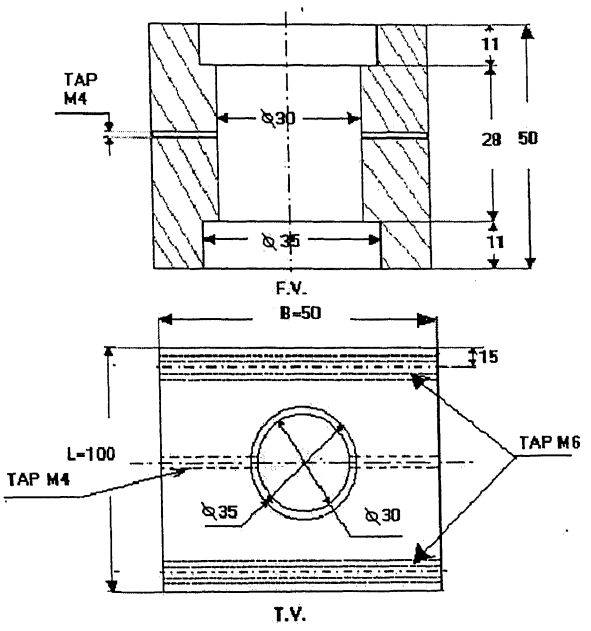

Figure 22: Bearing block - 2.

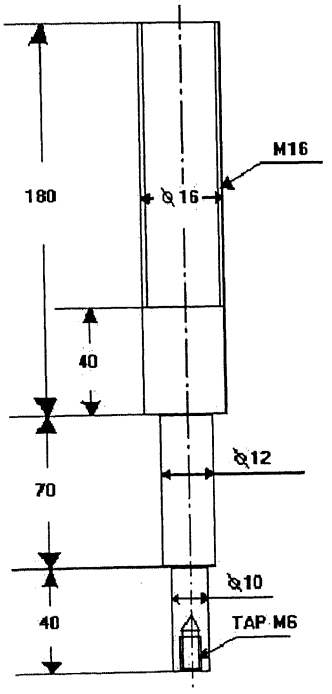

Figure 23: Shaft - 1.

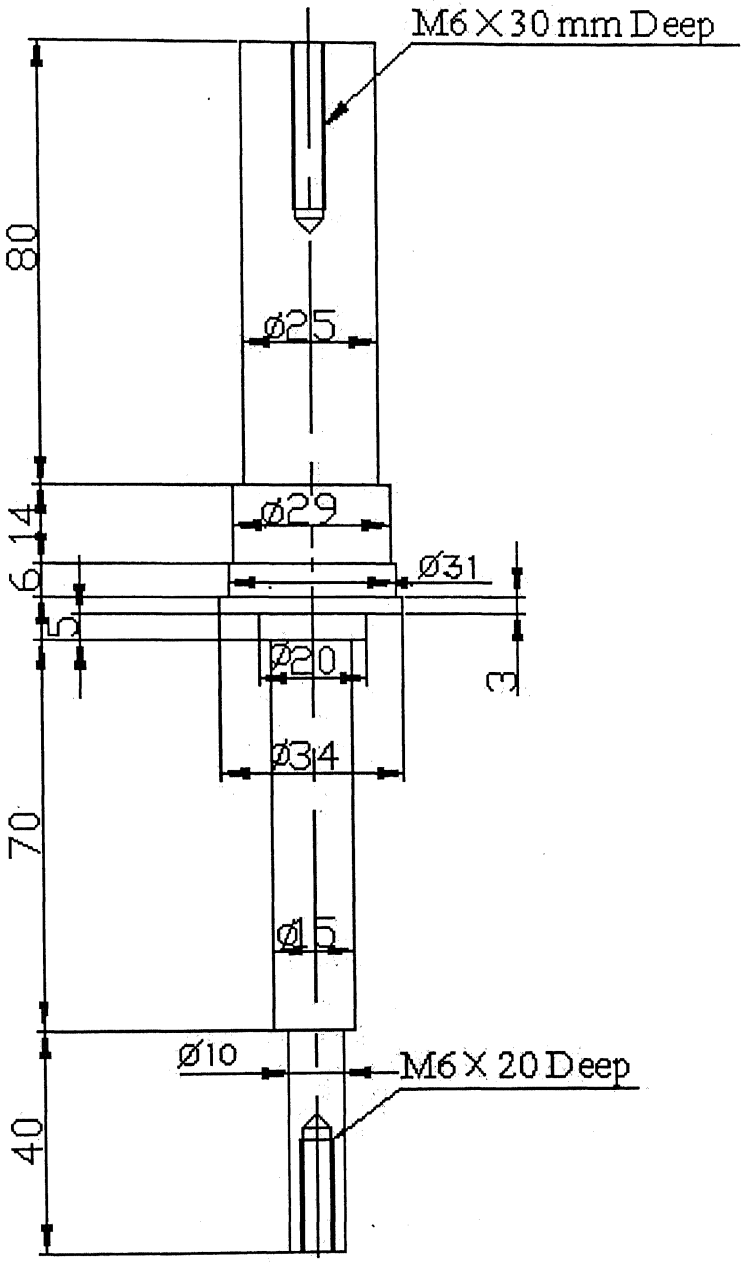

Figure 24: Shaft - 2.

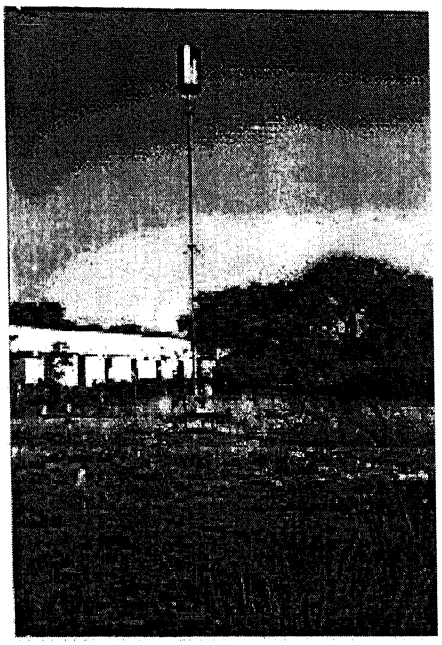

Figure 25: Field unit

Figure 26: Field unit Charging equipment

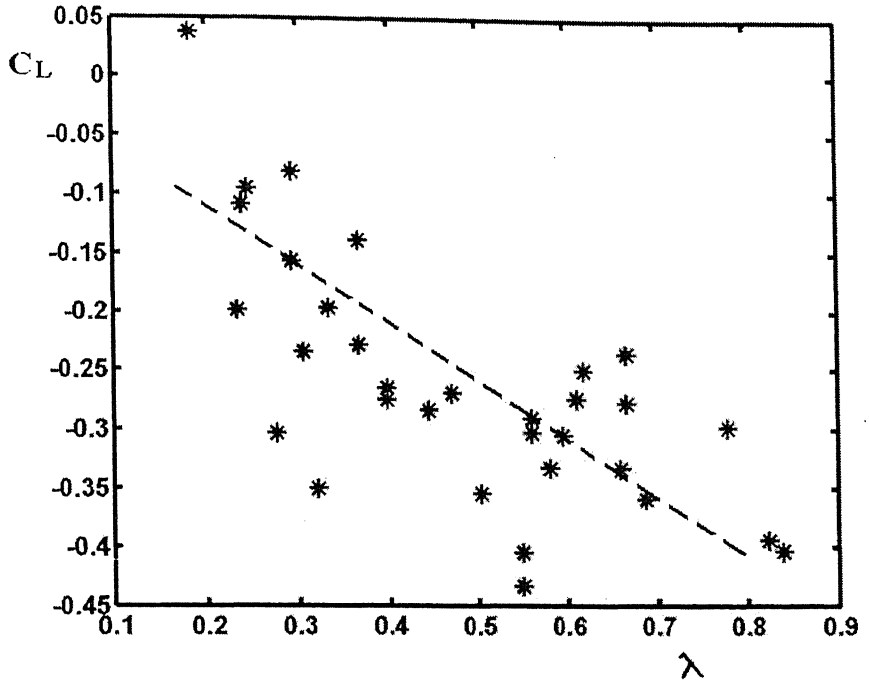

Fiqure 26(A) : Plot of C_L vs Lambda

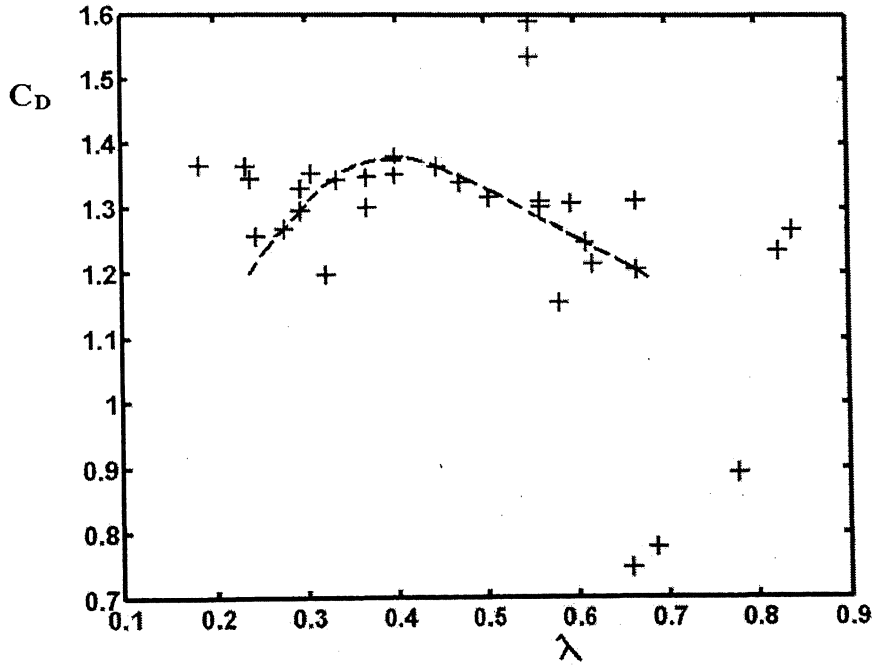

Figure 26(B) : Plot of C_D vs Lambda

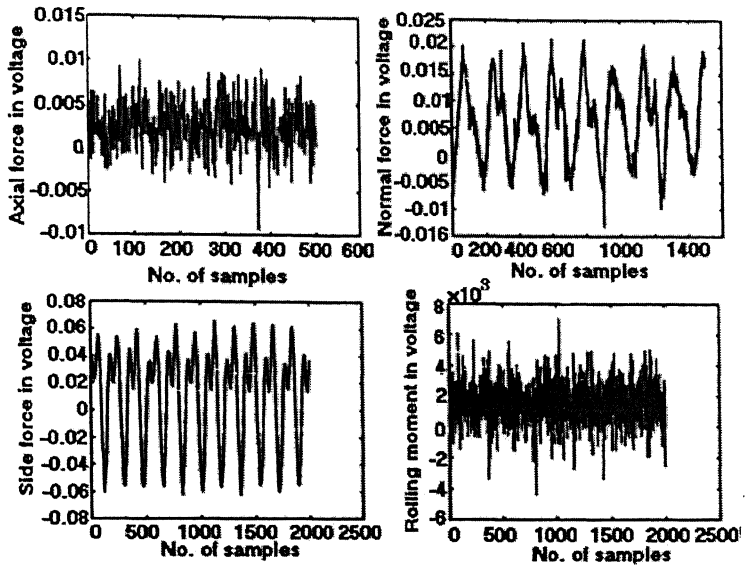

Figure 27: Voltage signals for different forces and moments for 1st round of expt. (Free rotation)

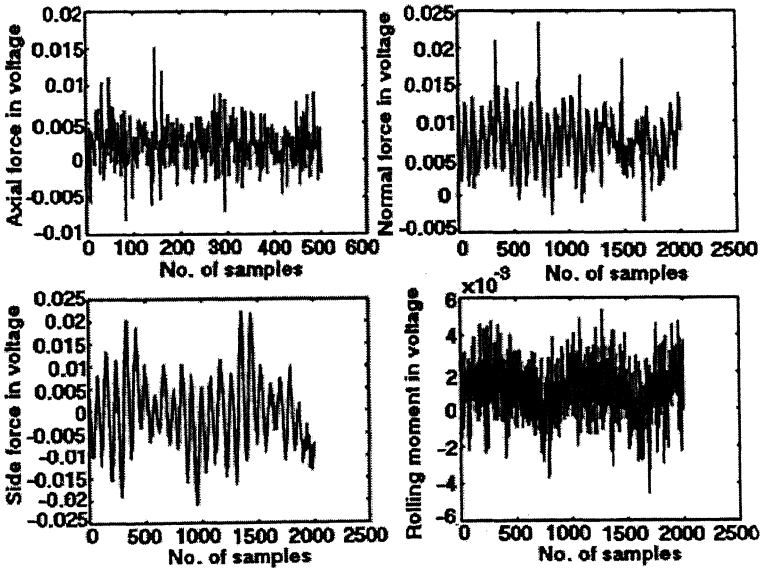

Figure 28: Voltage signals for different forces and moments for 1st round of expt. (Brake force applied)

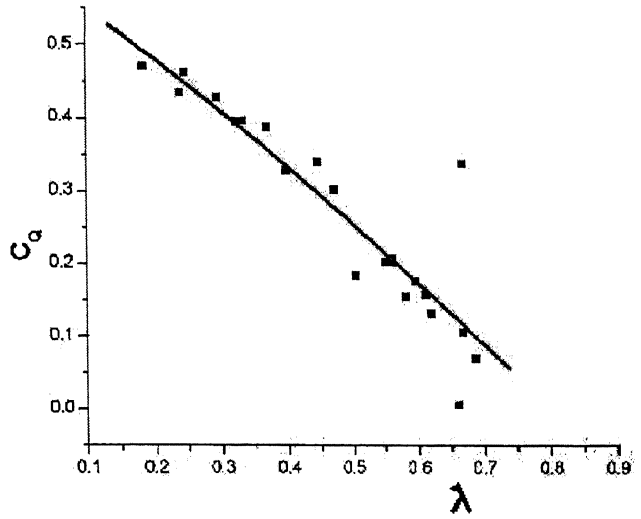

Figure 29: Plot of C_Q V/s λ for 1st round of expt.

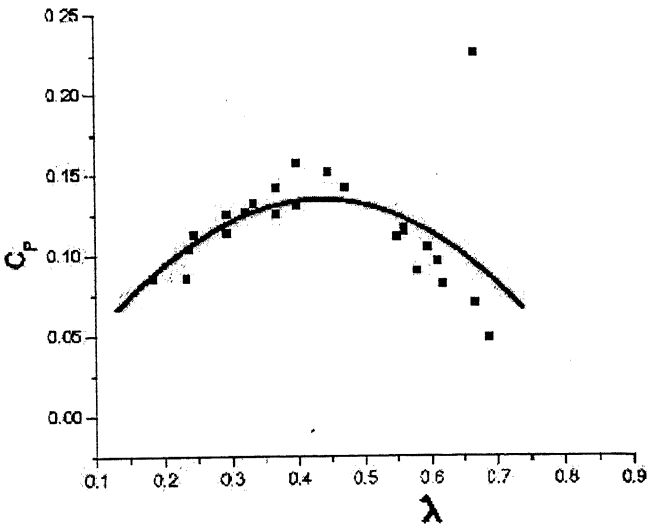

Figure 30: Plot of C_P V/s λ for 1st round of expt.

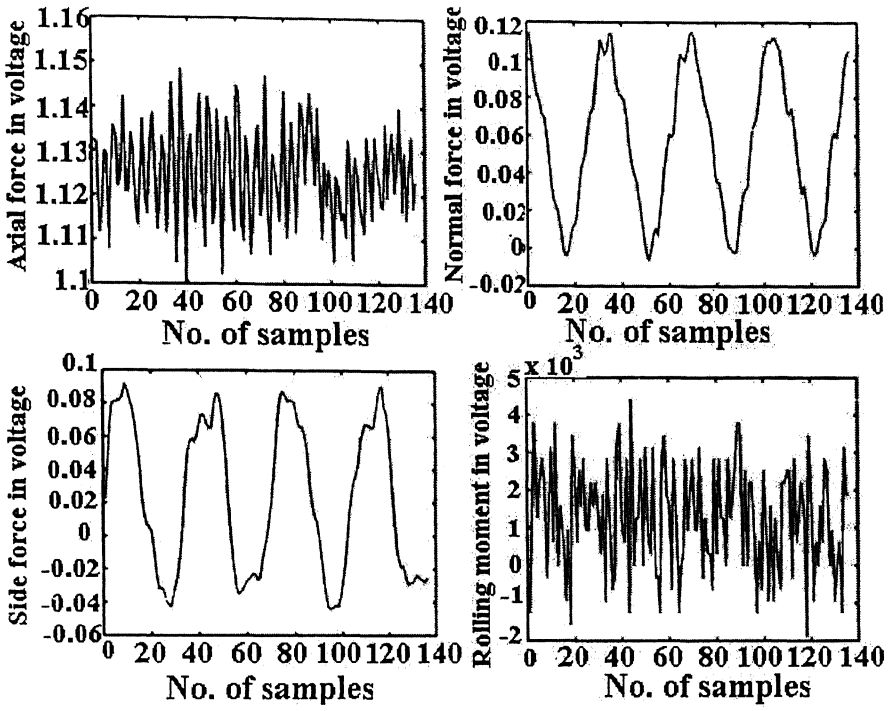

Figure 31: Voltage signals for different forces and moments at 8 m/s (Free rotation)

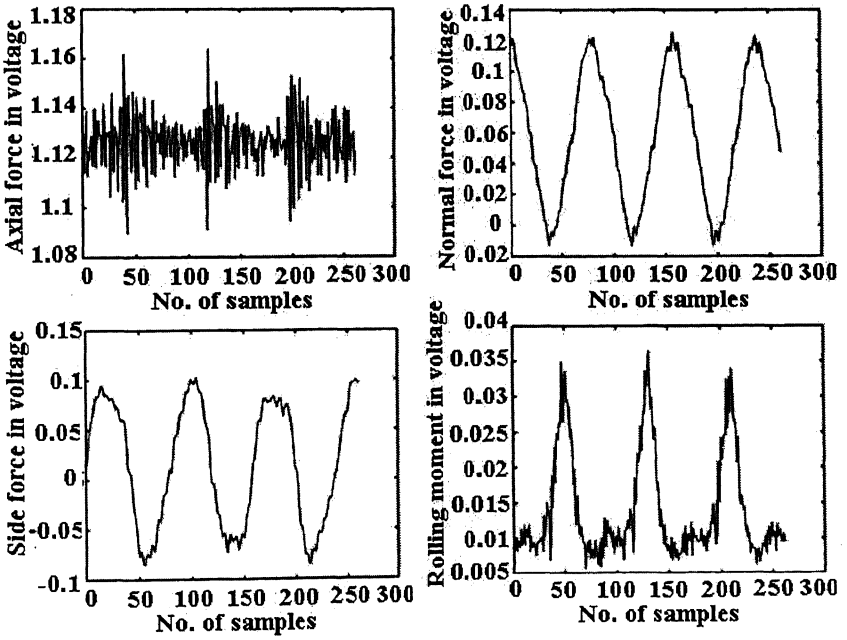

Figure 32: Voltage signals for different forces and moments at 8 m/s (Brake force applied)

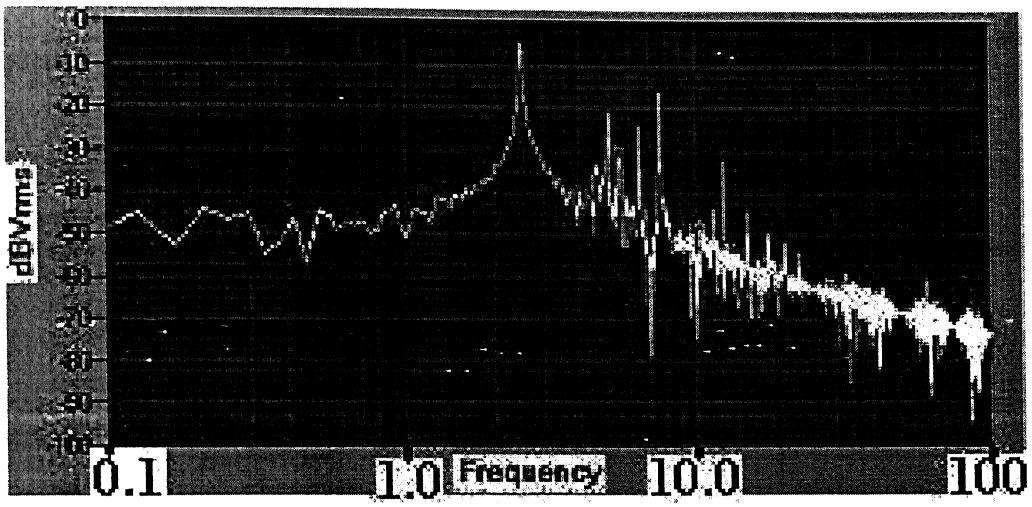

Figure 33: Power spectrum of drag

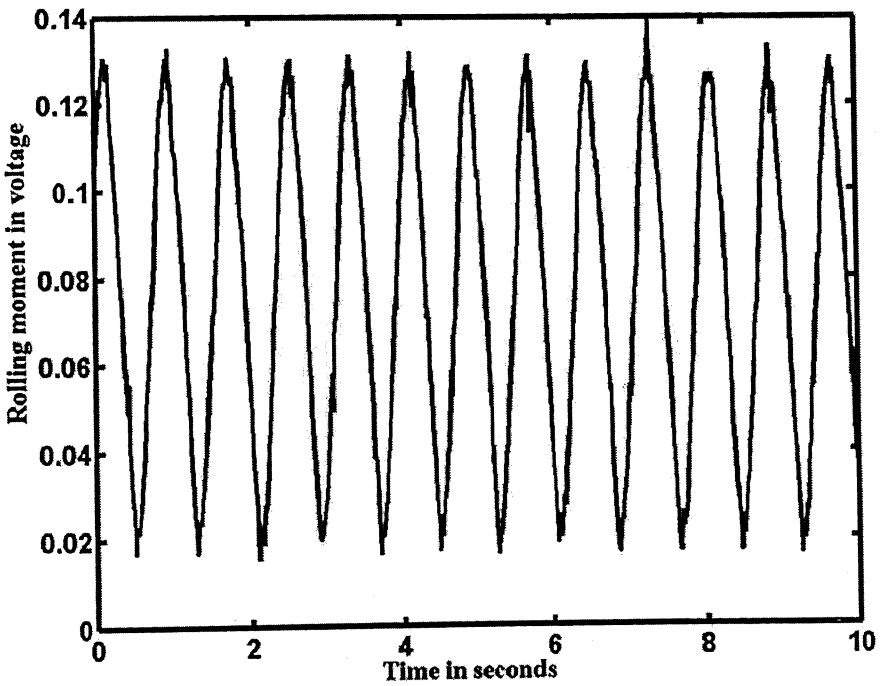

Figure 34: Torque Vs time

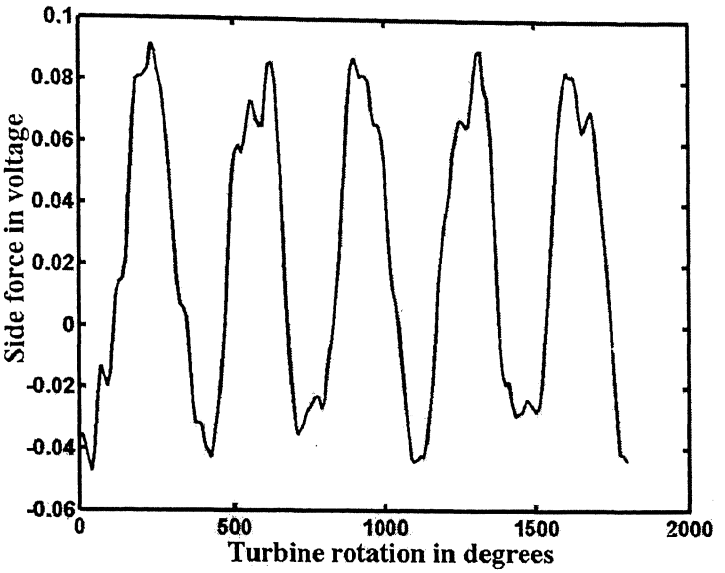

Figure 35: Variation of Side force Vs turbine rotation in degrees (free rotation)

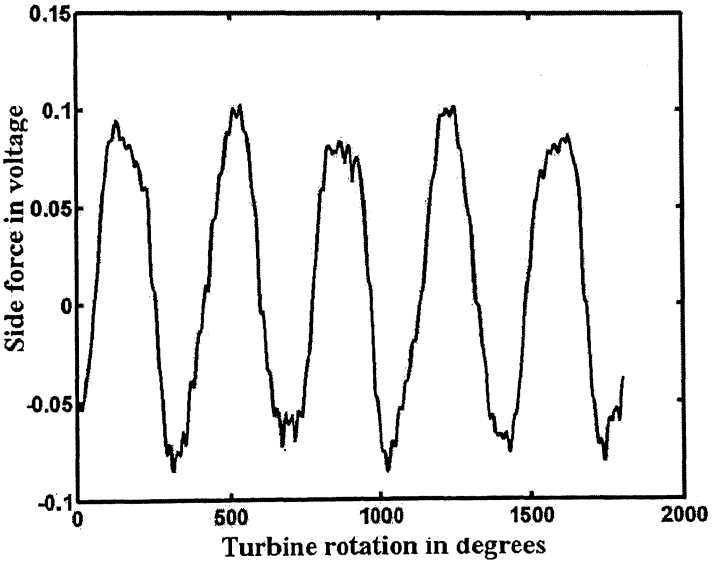

Figure 36: Variation of Side force Vs turbine rotation in degrees (Brake force applied)

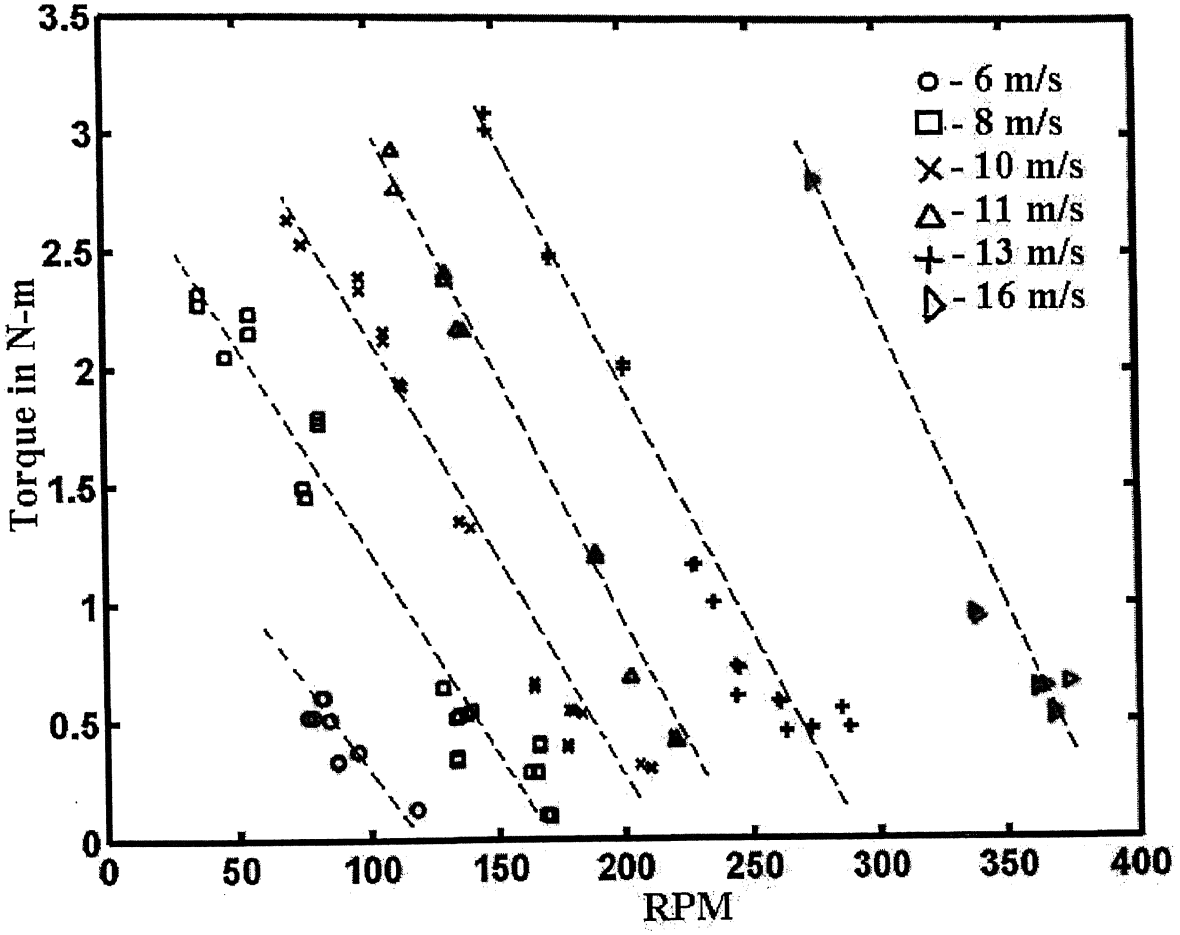

Figure 37: Variation of torque Vs rpm

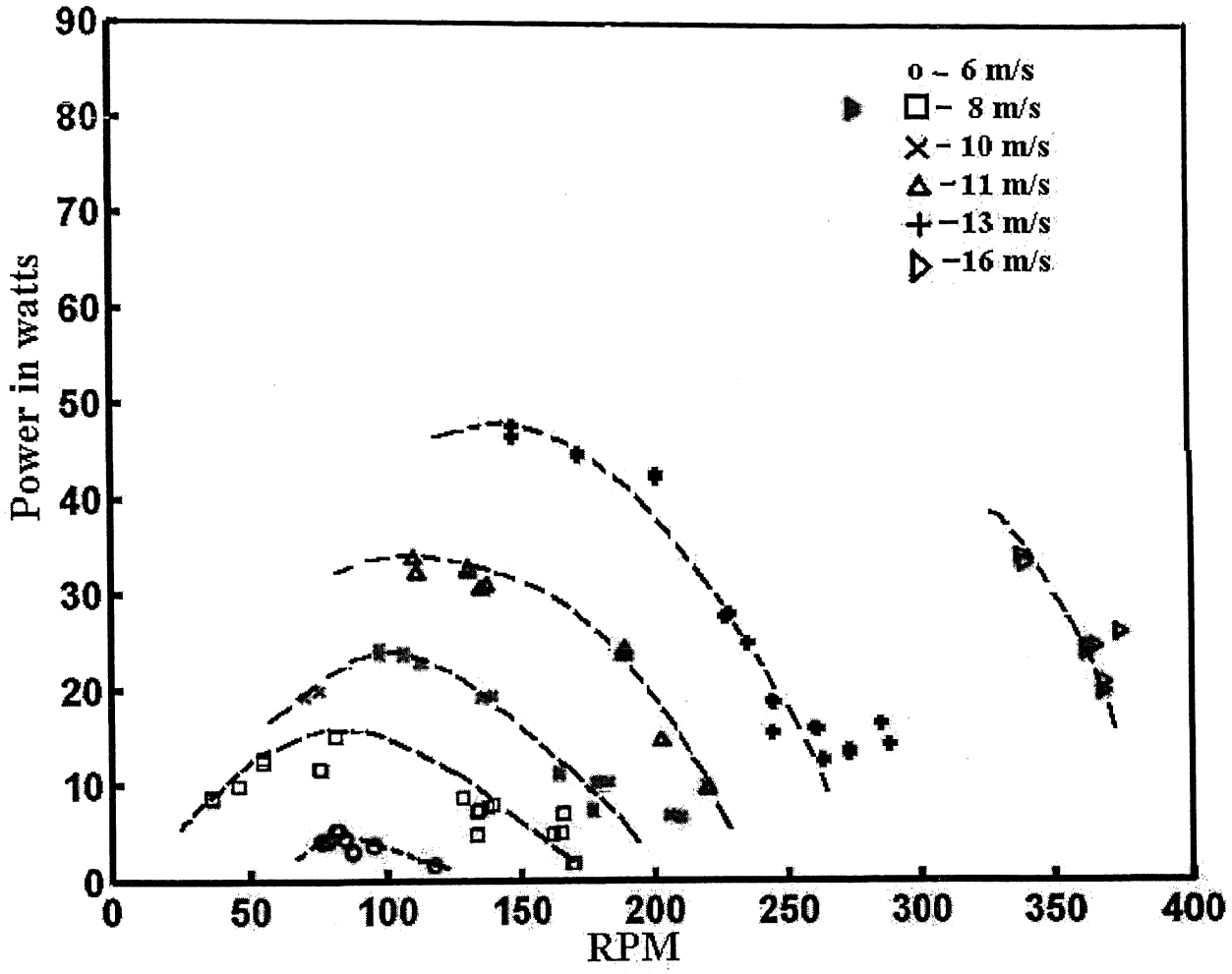

Figure 38: Variation of Power Vs RPM

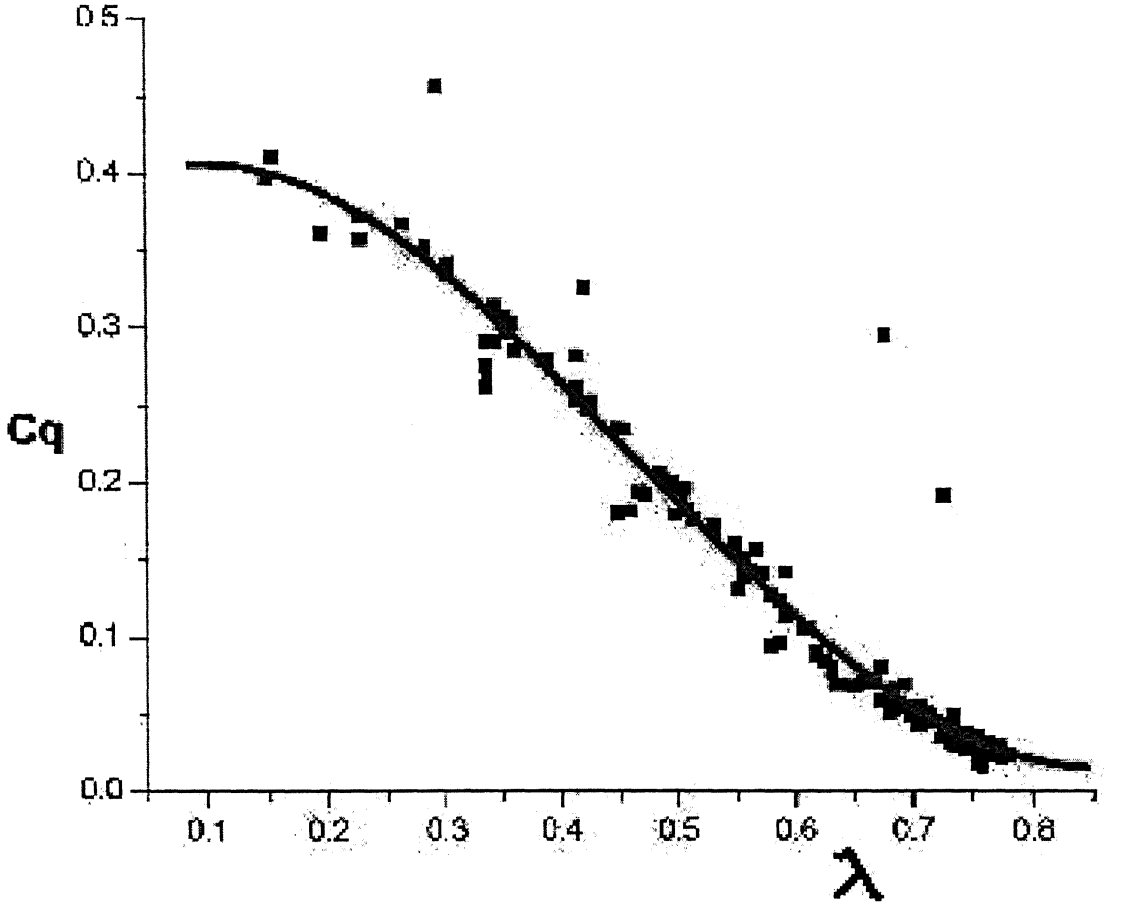

Figure 39: Plot of C_Q V/s λ for present experiment

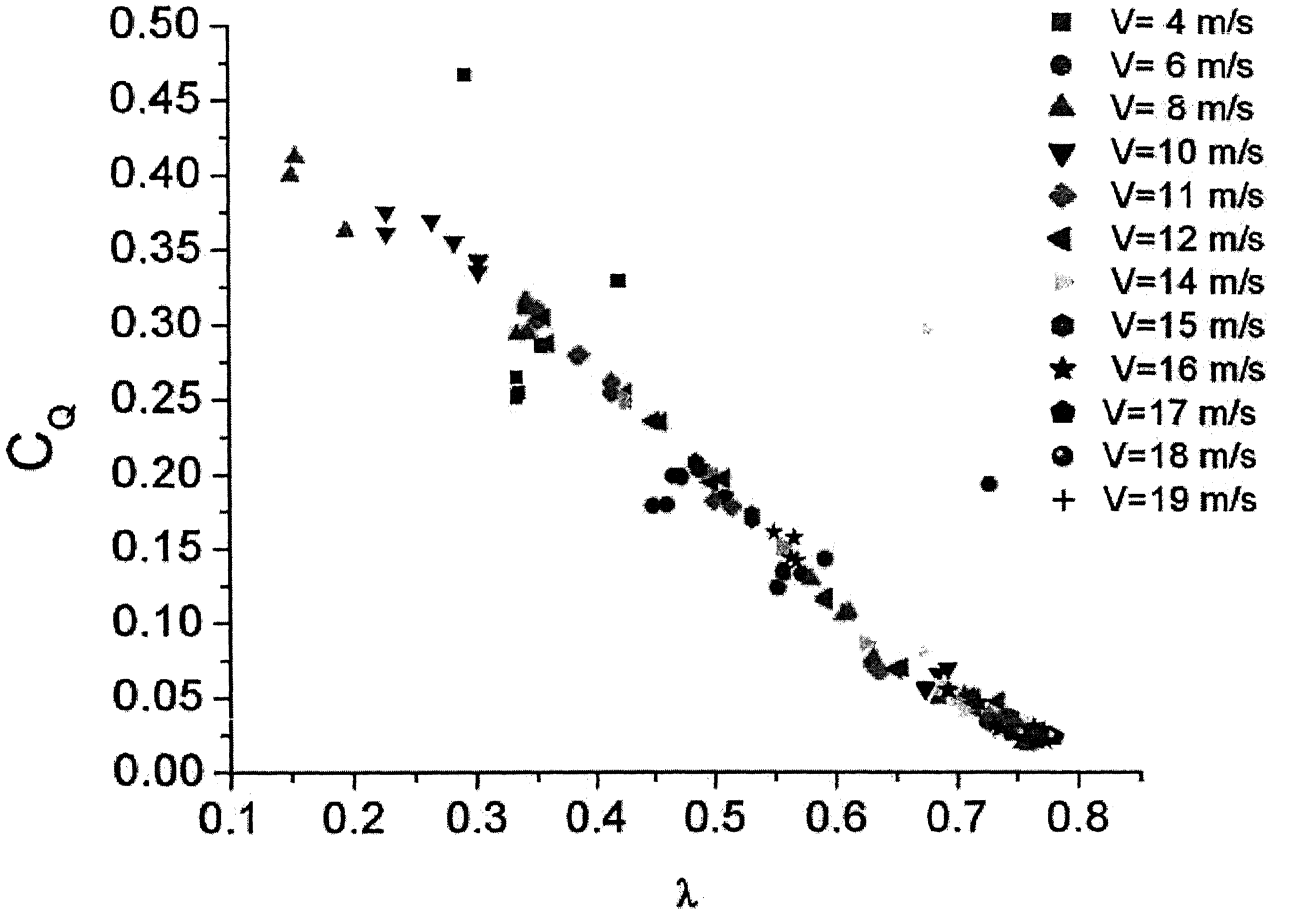

Figure 40: Plot of C_Q V/s λ for present experiment

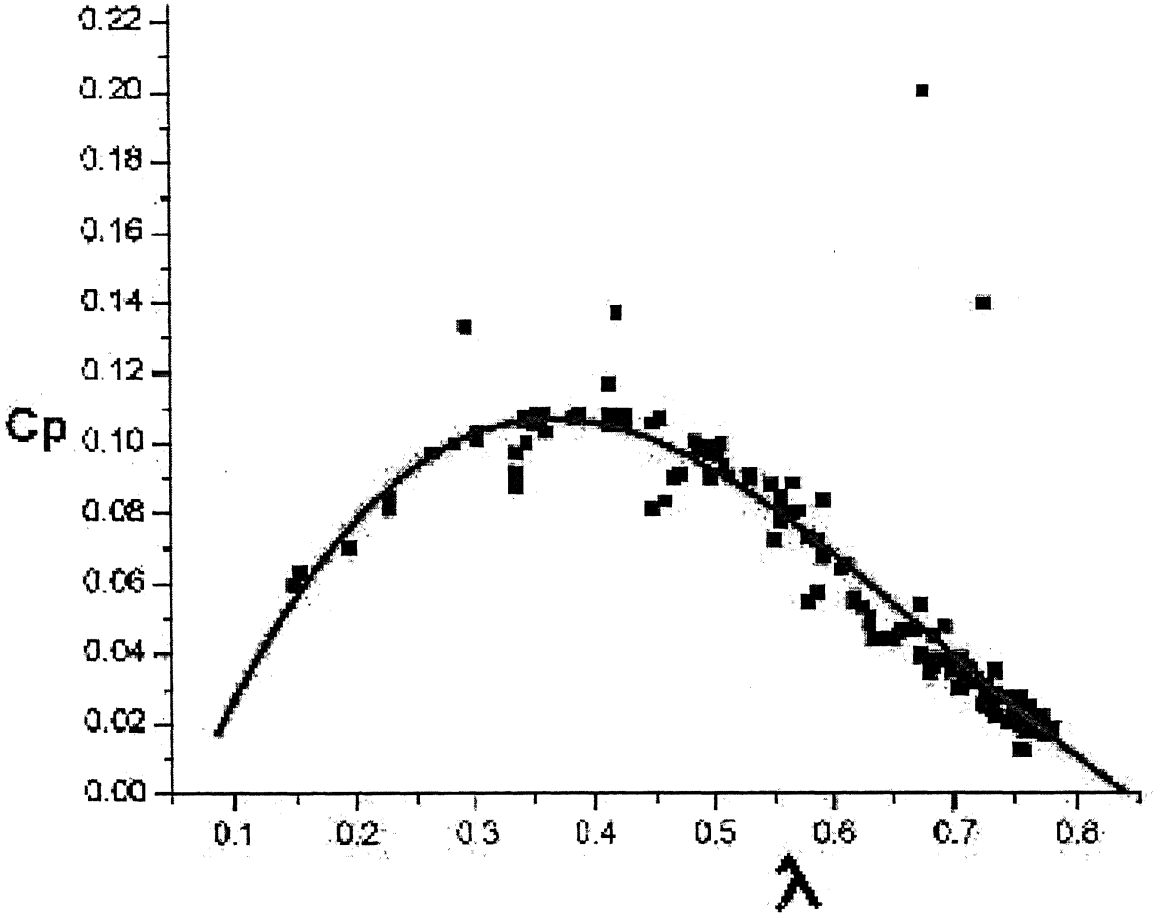

Figure 41: Plot of C_P V/s λ for present experiment

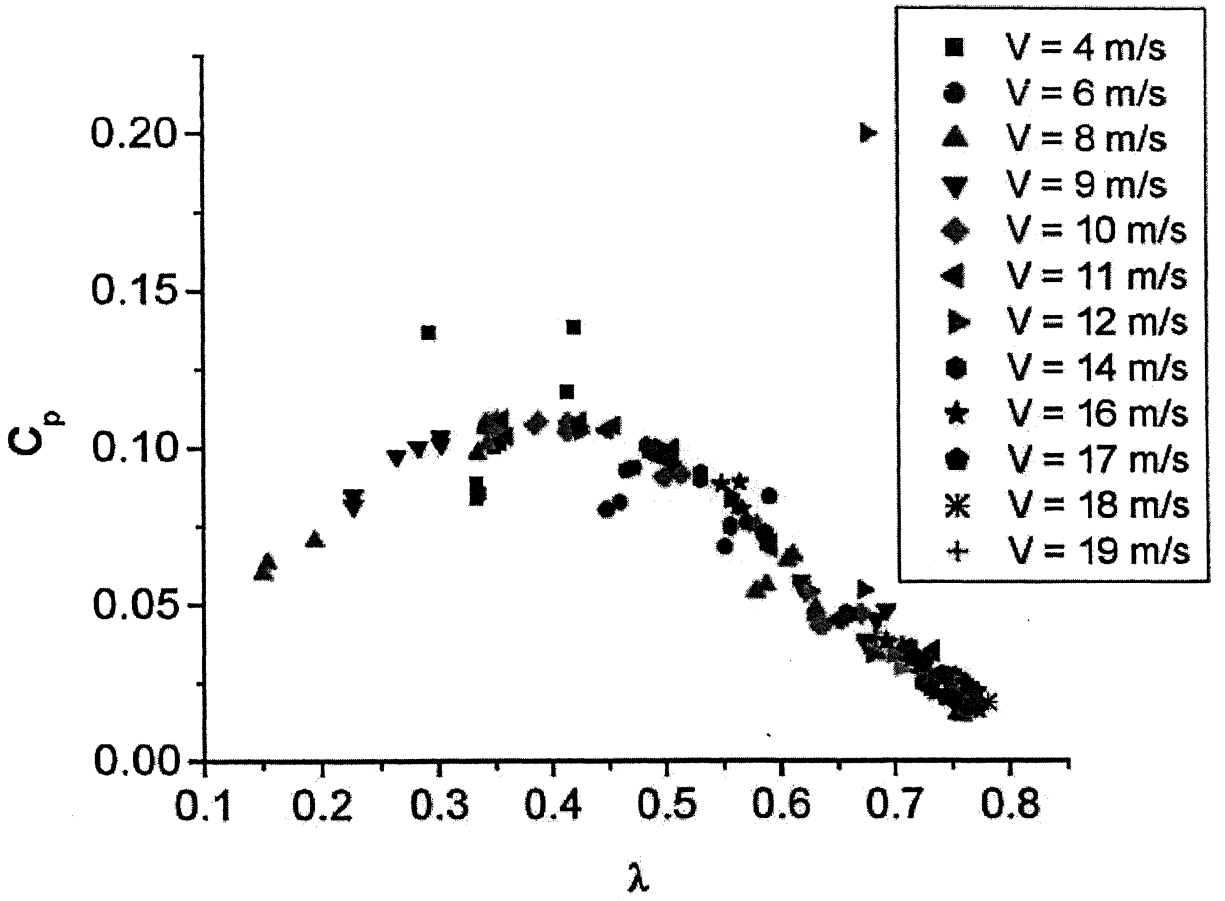

Figure 42: Plot of C_P V/s λ for present experiment

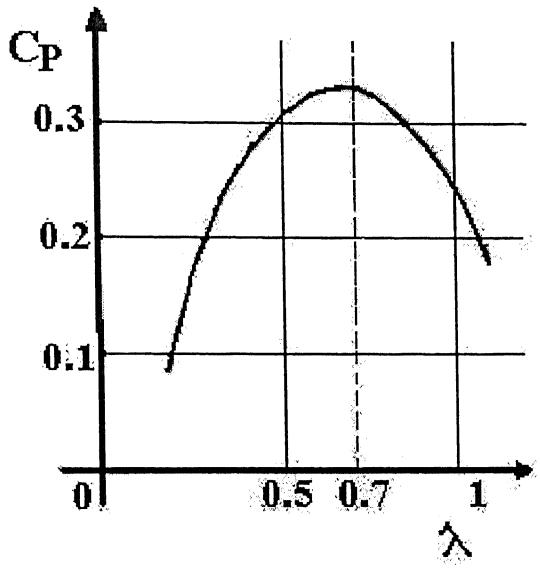

Figure 43: Plot of C_P vs λ given by Vinh and Houmaire

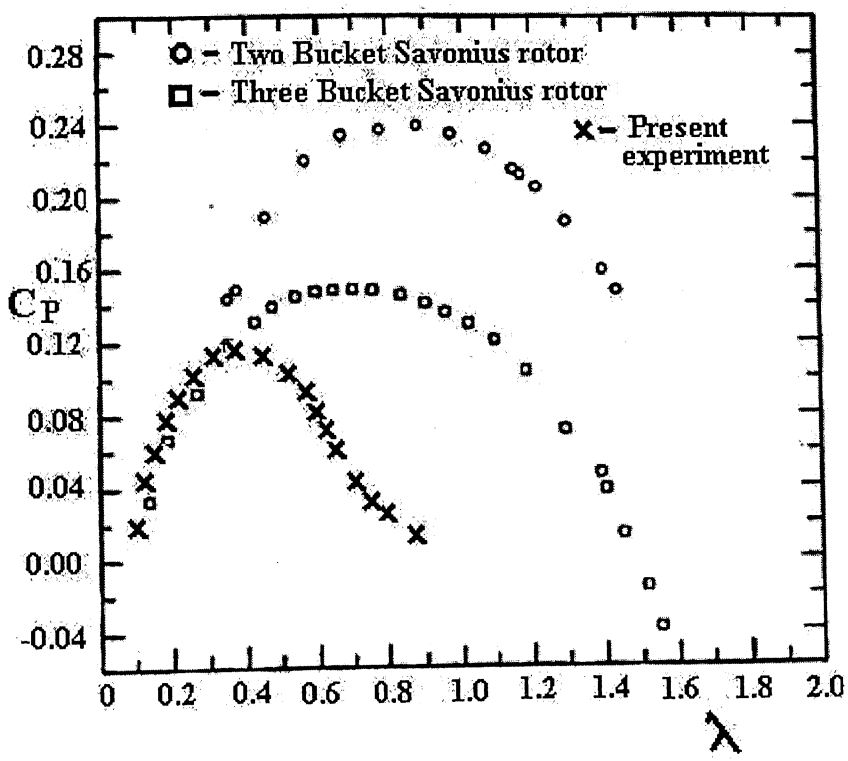

Figure 44: Plot of C_P vs λ for two and three blade Savonius rotor

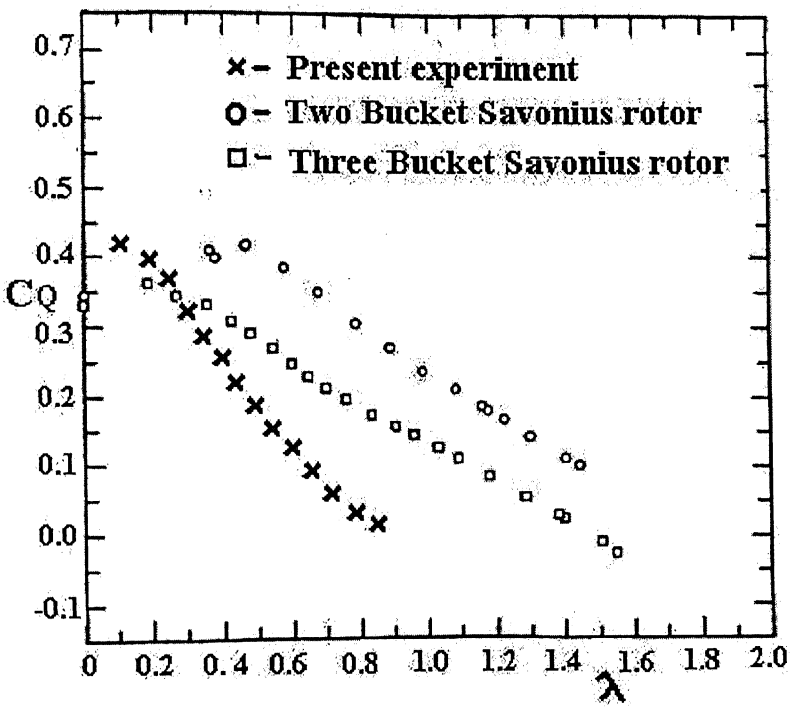

Figure 45: Plot of C_Q vs λ for two and three blade Savonius rotor

Important Results

Table 1: Table of lift and drag coefficient for 1st round of experiment

Drag force in N	Lift (side) force in N	Velocity in m/s	Coefficient of drag C_D	Coefficient of Lift C_L
3.063	-1.0233	4	0.893	-0.2983
2.5596	-1.1431	4	0.7462	-0.3333
2.669	-1.2301	4	0.7781	-0.3586
4.3497	-1.0423	4	1.2681	-0.3039
4.107	-1.2018	4	1.1974	-0.3504
4.5164	-1.2149	4	1.3167	-0.3542
5.4502	-1.4851	4	1.589	-0.433
5.266	-1.3874	4	1.5353	-0.4045
9.5243	-3.0406	6	1.2341	-0.394
9.7736	-3.1103	6	1.2664	-0.403
8.9134	-2.5664	6	1.155	-0.3325
10.0932	-2.3556	6	1.3078	-0.3052
10.4389	-2.0477	6	1.3526	-0.2653
10.6491	-2.1225	6	1.3799	-0.275
10.547	0.2875	6	1.3666	0.0373

Table 2: Table of lift and drag coefficient for 1st round of experiment

Drag force in N	Lift (side) force in N	Velocity in m/s	Coefficient of drag C_D	Coefficient of Lift C_L
9.7038	-0.7318	6	1.2574	-0.0948
14.3359	-2.9848	7	1.3648	-0.2841
14.077	-2.8309	7	1.3401	-0.2695
17.8748	-4.1534	8	1.3028	-0.3027
17.9787	-3.9846	8	1.3104	-0.2904
21.6798	-4.7618	9	1.2485	-0.2742
21.0895	-4.344	9	1.2145	-0.2502
25.8548	-5.9565	10	1.2061	-0.2779
28.1295	-5.0553	10	1.3122	-0.2358
28.9276	-4.8953	10	1.3494	-0.2284
27.8913	-2.9714	10	1.3011	-0.1386
27.7954	-3.346	10	1.2966	-0.1561
28.532	-1.7343	10	1.3309	-0.0809
28.8348	-2.3228	10	1.3451	-0.1084
35.4089	-5.1487	11	1.3651	-0.1985
34.8554	-5.094	11	1.3437	-0.1964
41.8066	-7.2433	12	1.3543	-0.2346

Appendix: Miscelleneous Tables

Table 3: Results of 1st round of experiment - I.

C_Q	λ	Power In watts	C_P	V_∞ in m/s	RPM	Torque (N-m)
0.0633	0.7791	0.6767	0.0493	4.0000	85.0000	0.076
0.0063	0.6600	0.0573	0.0042	4.0000	72.0000	0.0076
0.0717	0.6875	0.6765	0.0493	4.0000	75.0000	0.0861
0.2759	0.2750	1.0409	0.0759	4.0000	30.0000	0.3312
0.3962	0.3208	1.7438	0.1271	4.0000	35.0000	0.4756
0.1863	0.5041	1.2889	0.0939	4.0000	55.0000	0.2237
0.2042	0.5500	1.5406	0.1123	4.0000	60.0000	0.2451
0.0000	0.5500	0.0000	0.0000	4.0000	60.0000	0
0.1215	0.8250	4.6400	0.1002	6.0000	135.0000	0.3281
0.0541	0.8402	2.1030	0.0454	6.0000	137.5000	0.146
0.1560	0.5805	4.1937	0.0906	6.0000	95.0000	0.4214
0.1774	0.5958	4.8944	0.1057	6.0000	97.5000	0.4792
0.3303	0.3972	6.0758	0.1312	6.0000	65.0000	0.8923
0.3976	0.3972	7.3124	0.1579	6.0000	65.0000	1.0739
0.4715	0.1833	4.0025	0.0864	6.0000	30.0000	1.2736

Table 4: Results of 1st round of experiment - II.

C_Q	λ	Power In watts	C_P	V_∞ in m/s	RPM	Torque (N-m)
0.4640	0.2444	5.2517	0.1134	6.0000	40.0000	1.2533
0.3420	0.4452	11.1954	0.1523	7.0000	85.0000	1.2573
0.3034	0.4714	10.5180	0.1430	7.0000	90.0000	1.1156
0.2045	0.5614	12.6004	0.1148	8.0000	122.5000	0.9819
0.2101	0.5614	12.9456	0.1179	8.0000	122.5000	1.0088
0.1585	0.6111	15.1352	0.0968	9.0000	150.0000	0.9632
0.1332	0.6192	12.8929	0.0825	9.0000	152.0000	0.8097
0.1064	0.6673	15.2202	0.0710	10.0000	182.0000	0.7983
0.3410	0.6673	48.7796	0.2275	10.0000	182.0000	2.5585
0.3445	0.3666	27.0754	0.1263	10.0000	100.0000	2.5846
0.3888	0.3666	30.5607	0.1426	10.0000	100.0000	2.9173
0.3908	0.2933	24.5751	0.1146	10.0000	80.0000	2.9324
0.4288	0.2933	26.9602	0.1258	10.0000	80.0000	3.217
0.4358	0.2383	22.2667	0.1039	10.0000	65.0000	3.2701
0.3681	0.2333	24.5046	0.0859	11.0000	70.0000	3.3417
0.3977	0.3333	37.8203	0.1325	11.0000	100.0000	3.6103
0.3080	0.3055	34.8599	0.0941	12.0000	100.0000	3.3277

Table 5: Results of 2nd round of experiment - I.

V_∞ in m/s	RPM	Torque (N-m)	λ	Power In watts	C_P	C_Q
4.1697	38	0.3299	0.3344	1.3141	0.0846	0.2529
3.9312	38	0.3331	0.3547	1.3268	0.1019	0.2872
4.1697	38	0.3469	0.3344	1.382	0.0889	0.2659
5.7307	87	0.3327	0.557	3.0342	0.0752	0.135
5.7307	87	0.3368	0.557	3.0719	0.0761	0.1367
7.7386	133	0.3354	0.6306	4.6761	0.0471	0.0746
7.7386	133	0.3502	0.6306	4.8831	0.0492	0.0779
9.6295	177	0.3907	0.6744	7.2494	0.0379	0.0562
9.6295	177	0.4037	0.6744	7.4913	0.0391	0.058
11.2915	220	0.4139	0.7149	9.547	0.0309	0.0433
11.2915	220	0.4233	0.7149	9.7616	0.0316	0.0442
13.0384	263	0.4592	0.7401	12.6618	0.0266	0.036
13.1122	263	0.4565	0.7359	12.5867	0.026	0.0354
14.1059	288	0.4734	0.7491	14.2929	0.0238	0.0317
14.1059	288	0.4691	0.7491	14.1617	0.0235	0.0314
15.1619	313	0.4713	0.7575	15.4651	0.0207	0.0273
15.2255	313	0.427	0.7543	14.0115	0.0185	0.0246
16.2683	343	0.4189	0.7736	15.0613	0.0163	0.0211
17.5809	368	0.5414	0.768	20.8858	0.0179	0.0233
17.6358	368	0.5167	0.7656	19.9336	0.017	0.0221
14.4442	304	0.3826	0.7722	12.1926	0.0189	0.0244

Table 6: Results of 2nd round of experiment - II.

V_∞ in m/s	RPM	Torque (N-m)	λ	Power In watts	C_P	C_Q
14.5773	304	0.3616	0.7652	11.5249	0.0174	0.0227
12.6625	261	0.3063	0.7563	8.3805	0.0193	0.0255
12.6625	261	0.3185	0.7563	8.715	0.02	0.0265
10.4935	210	0.2999	0.7343	6.6021	0.0267	0.0363
10.401	206	0.3175	0.7267	6.8569	0.0284	0.0391
8.5679	165	0.2863	0.7066	4.9525	0.0367	0.052
8.6799	162	0.2848	0.6848	4.8375	0.0345	0.0504
5.383	81	0.2718	0.5521	2.3076	0.069	0.125
5.2005	81	0.2734	0.5715	2.3217	0.077	0.1347
3.9312	36	0.2959	0.336	1.1166	0.0857	0.2552
3.6773	35	0.2927	0.3492	1.0739	0.1007	0.2885
6.3693	128	-0.3141	0.7374	-4.2144	-0.0761	-0.1032
6.3693	125	-0.3083	0.7201	-4.0396	-0.0729	-0.1013
6.2158	78	0.5244	0.4604	4.2877	0.0833	0.1809
6.2158	76	0.5222	0.4486	4.1604	0.0808	0.1801
8.6799	137	0.5315	0.5791	7.6342	0.0545	0.094
8.6799	139	0.546	0.5876	7.9555	0.0567	0.0966
10.3077	178	0.5508	0.6336	10.2779	0.0438	0.0691
10.3077	179	0.5487	0.6372	10.2965	0.0439	0.0688
12.1963	226	0.5739	0.6799	13.5976	0.035	0.0514
12.1963	226	0.5641	0.6799	13.3653	0.0344	0.0505

Table 7: Results of 2nd round of experiment - III.

V_∞ in m/s	RPM	Torque (N-m)	λ	Power In watts	C_P	C_Q
13.547	261	0.5823	0.7069	15.9334	0.0299	0.0423
13.547	260	0.5874	0.7042	16.0097	0.03	0.0427
15.034	298	0.6007	0.7273	18.7671	0.0258	0.0354
15.0981	298	0.5918	0.7242	18.4867	0.0251	0.0346
16.7365	335	0.6331	0.7344	22.2345	0.0221	0.0301
16.7365	336	0.6249	0.7366	22.0105	0.0219	0.0297
18.2283	374	0.668	0.7528	26.1902	0.0202	0.0268
18.2283	375	0.6509	0.7548	25.5868	0.0197	0.0261
19.359	400	0.646	0.7581	27.0872	0.0174	0.023
19.359	400	0.6514	0.7581	27.3168	0.0176	0.0232
17.8535	365	0.6452	0.7501	24.6874	0.0202	0.027
17.8535	362	0.6477	0.744	24.5793	0.0201	0.0271
15.9081	317	0.6132	0.7312	20.3795	0.0236	0.0323
15.9081	317	0.6055	0.7312	20.1208	0.0233	0.0319
14.9696	298	0.5944	0.7304	18.5684	0.0258	0.0354
15.034	298	0.581	0.7273	18.1513	0.0249	0.0343
12.8142	244	0.6068	0.6987	15.5203	0.0344	0.0492
12.7386	235	3.6409	0.6769	89.6964	0.2024	0.299
12.8142	235	1.0122	0.6729	24.9367	0.0553	0.0822
6.0584	117	0.1335	0.7086	1.6371	0.0343	0.0485
5.8968	117	0.5089	0.728	6.2425	0.142	0.1951
6.0584	84	0.5125	0.5087	4.5131	0.0947	0.1861

Table 8: Results of 2nd round of experiment - IV.

V_∞ in m/s	RPM	Torque (N-m)	λ	Power In watts	C_P	C_Q
7.9843	133	0.5195	0.6112	7.2435	0.0664	0.1086
8.1044	134	0.5279	0.6067	7.4156	0.065	0.1071
10.0227	183	0.536	0.6699	10.2828	0.0476	0.0711
10.0227	183	0.538	0.6699	10.3219	0.0478	0.0714
11.8753	230	0.5421	0.7106	13.0704	0.0364	0.0512
11.8753	231	0.5326	0.7137	12.8972	0.0359	0.0503
14.1059	285	0.5666	0.7413	16.9291	0.0281	0.038
14.0372	285	0.5546	0.745	16.5705	0.0279	0.0375
15.6633	325	0.6084	0.7613	20.7302	0.0252	0.0331
15.6633	326	0.5829	0.7637	19.9201	0.0242	0.0317
17.2481	362	0.648	0.7701	24.5924	0.0224	0.029
17.2481	362	0.6345	0.7701	24.0794	0.0219	0.0284
18.7507	399	0.6386	0.7808	26.7098	0.0189	0.0242
18.7507	399	0.6371	0.7808	26.6475	0.0189	0.0241
15.7862	332	0.5481	0.7717	19.0755	0.0226	0.0293
15.7862	332	0.534	0.7717	18.5853	0.022	0.0286
13.2587	273	0.4762	0.7555	13.6296	0.0273	0.0361
13.3314	273	0.4646	0.7514	13.2958	0.0262	0.0348
10.944	219	0.4299	0.7342	9.8694	0.0351	0.0478
10.944	219	0.4377	0.7342	10.0485	0.0358	0.0487
8.8997	166	0.3977	0.6844	6.9203	0.0458	0.0669

Table 9: Results of 2nd round of experiment - V.

V_∞ in m/s	RPM	Torque (N-m)	λ	Power In watts	C_P	C_Q
8.7905	166	0.4074	0.6929	7.0899	0.0487	0.0703
5.8968	95	0.3769	0.5911	3.754	0.0854	0.1445
4.1697	47	0.3734	0.4136	1.8399	0.1184	0.2863
3.9312	45	0.3842	0.42	1.8125	0.1392	0.3313
8.2227	169	0.1008	0.7541	1.7863	0.015	0.0199
8.2227	170	0.0976	0.7586	1.7393	0.0146	0.0192
8.1044	76	1.4568	0.3441	11.6071	0.1017	0.2956
8.2227	75	1.4969	0.3347	11.7691	0.0987	0.2951
9.9258	135	1.3552	0.499	19.1796	0.0915	0.1833
9.9258	139	1.329	0.5138	19.3667	0.0924	0.1798
11.7114	189	1.2214	0.5921	24.1993	0.0703	0.1187
11.71	189	1.201	0.5922	23.7955	0.0691	0.1167
11.7114	189	1.1967	0.5921	23.7098	0.0689	0.1163
13.3314	227	1.1661	0.6248	27.751	0.0546	0.0875
13.4036	228	1.1713	0.6241	27.9963	0.0542	0.0869
14.7748	265	1.1922	0.6581	33.1213	0.0479	0.0728
14.7748	266	1.1743	0.6606	32.7471	0.0474	0.0717
16.3275	308	1.1202	0.6921	36.1693	0.0388	0.056
16.3275	309	1.1081	0.6944	35.8949	0.0385	0.0554
18.2283	356	1.1526	0.7166	43.0151	0.0331	0.0462
18.2283	358	1.1518	0.7206	43.2293	0.0333	0.0462

Table 10: Results of 2nd round of experiment - VI

V_∞ in m/s	RPM	Torque (N-m)	λ	Power In watts	C_P	C_Q
17.0793	338	0.9687	0.7261	34.3238	0.0321	0.0443
17.1358	339	0.9432	0.7259	33.5189	0.0311	0.0428
15.4147	301	0.8427	0.7165	26.5908	0.0339	0.0473
15.4147	302	0.8336	0.7189	26.3912	0.0336	0.0468
13.0384	244	0.7381	0.6866	18.8811	0.0397	0.0579
13.0384	245	0.7298	0.6895	18.7439	0.0394	0.0572
11.4614	203	0.6903	0.6499	14.69	0.0455	0.07
11.3768	203	0.6914	0.6547	14.7142	0.0466	0.0712
9.7293	164	0.6478	0.6185	11.1378	0.0564	0.0912
9.7293	164	0.6678	0.6185	11.4819	0.0582	0.094
8.1044	128	0.6466	0.5795	8.6759	0.076	0.1312
8.1044	128	0.6462	0.5795	8.6711	0.076	0.1311
6.3693	82	0.607	0.4724	5.2177	0.0942	0.1994
6.3693	81	0.6093	0.4666	5.1738	0.0934	0.2002
4.3952	35	0.6796	0.2922	2.4936	0.137	0.4689
8.7905	36	2.3205	0.1503	8.7574	0.0601	0.4002
9.7293	75	2.5308	0.2828	19.8988	0.1008	0.3563
9.7293	70	2.6343	0.264	19.331	0.0979	0.3709
11.2915	111	2.765	0.3607	32.1743	0.1042	0.289
11.2915	110	2.9298	0.3574	33.7859	0.1095	0.3063
12.7	147	3.0211	0.4247	46.5571	0.106	0.2496

Table 11: Results of 2nd round of experiment - VII.

V_∞ in m/s	RPM	Torque (N-m)	λ	Power In watts	C_P	C_Q
12.7386	147	3.0927	0.4234	47.6595	0.1076	0.254
14.2422	188	3.19	0.4843	62.8699	0.1015	0.2096
14.2422	189	3.1187	0.4869	61.7933	0.0998	0.2049
18.2283	356	1.1526	0.7166	43.0151	0.0331	0.0462
18.2283	358	1.1518	0.7206	43.2293	0.0333	0.0462
17.0793	338	0.9687	0.7261	34.3238	0.0321	0.0443
17.1358	339	0.9432	0.7259	33.5189	0.0311	0.0428
15.4147	301	0.8427	0.7165	26.5908	0.0339	0.0473
15.4147	302	0.8336	0.7189	26.3912	0.0336	0.0468
13.0384	244	0.7381	0.6866	18.8811	0.0397	0.0579
13.0384	245	0.7298	0.6895	18.7439	0.0394	0.0572
11.4614	203	0.6903	0.6499	14.69	0.0455	0.07
11.3768	203	0.6914	0.6547	14.7142	0.0466	0.0712
9.7293	164	0.6478	0.6185	11.1378	0.0564	0.0912
9.7293	164	0.6678	0.6185	11.4819	0.0582	0.094
8.1044	128	0.6466	0.5795	8.6759	0.076	0.1312
8.1044	128	0.6462	0.5795	8.6711	0.076	0.1311
6.3693	82	0.607	0.4724	5.2177	0.0942	0.1994
6.3693	81	0.6093	0.4666	5.1738	0.0934	0.2002
4.3952	35	0.6796	0.2922	2.4936	0.137	0.4689
8.7905	36	2.3205	0.1503	8.7574	0.0601	0.4002

Table 12: Results of 2nd round of experiment - VIII

V_∞ in m/s	RPM	Torque (N-m)	λ	Power In watts	C_P	C_Q
9.7293	75	2.5308	0.2828	19.8988	0.1008	0.3563
9.7293	70	2.6343	0.264	19.331	0.0979	0.3709
11.2915	111	2.765	0.3607	32.1743	0.1042	0.289
11.2915	110	2.9298	0.3574	33.7859	0.1095	0.3063
12.7	147	3.0211	0.4247	46.5571	0.106	0.2496
12.7386	147	3.0927	0.4234	47.6595	0.1076	0.254
14.2422	188	3.19	0.4843	62.8699	0.1015	0.2096
14.2422	189	3.1187	0.4869	61.7933	0.0998	0.2049
15.9081	238	3.0873	0.5489	77.029	0.0893	0.1626
15.96	246	3.0364	0.5655	78.3047	0.0898	0.1589
15.9687	245	2.7829	0.5629	71.4769	0.0819	0.1455
17.2481	276	2.7983	0.5871	80.9662	0.0736	0.1254
17.304	276	2.821	0.5852	81.6216	0.0735	0.1256
15.8472	245	2.6994	0.5673	69.3315	0.0813	0.1433
15.9081	246	2.722	0.5674	70.1975	0.0813	0.1434
14.1742	205	2.6325	0.5307	56.5757	0.0927	0.1746
14.1742	205	2.5804	0.5307	55.4543	0.0908	0.1712
12.8142	172	2.491	0.4925	44.9168	0.0996	0.2022
12.7386	172	2.4769	0.4954	44.6609	0.1008	0.2034
11.2057	130	2.3806	0.4257	32.4442	0.1076	0.2527
11.2	130	2.41	0.4259	32.8446	0.1091	0.2561
10.1186	97	2.3356	0.3517	23.7499	0.1069	0.304

Table 13: Results of 2nd round of experiment - IX

V_∞ in m/s	RPM	Torque (N-m)	λ	Power In watts	C_P	C_Q
10.1186	97	2.3913	0.3517	24.3166	0.1095	0.3113
8.8997	55	2.233	0.2268	12.8752	0.0852	0.3758
8.8997	55	2.1507	0.2268	12.4004	0.0821	0.3619
8.6799	81	1.7678	0.3424	15.0112	0.1071	0.3127
8.6799	81	1.7917	0.3424	15.2143	0.1085	0.317
10.0227	113	1.929	0.4137	22.8518	0.1059	0.2559
9.9258	112	1.9452	0.414	22.8396	0.1089	0.2631
11.7936	162	2.0225	0.504	34.3489	0.0977	0.1938
11.7936	162	2.0159	0.504	34.2365	0.0974	0.1932
13.2587	201	2.0054	0.5562	42.2563	0.0846	0.152
13.2587	201	2.0264	0.5562	42.6985	0.0855	0.1536
11.7936	163	2.0724	0.5071	35.4132	0.1007	0.1986
11.8753	161	2.077	0.4975	35.0565	0.0976	0.1963
11.0319	137	2.1616	0.4557	31.0454	0.1079	0.2367
11.0319	135	2.168	0.449	30.6824	0.1066	0.2374
10.0227	106	2.1217	0.3881	23.5766	0.1092	0.2815
10.1186	106	2.1581	0.3844	23.9814	0.108	0.2809
9.2195	76	2.1468	0.3025	17.1043	0.1018	0.3366
9.2195	76	2.194	0.3025	17.4806	0.1041	0.344
8.6799	46	2.0521	0.1945	9.8959	0.0706	0.363
8.5679	36	2.2724	0.1542	8.576	0.0636	0.4126